

**We could like to thank all four reviewers for their critical comments, which we think tremendously helped to improve the quality and clarity of this manuscript. We hope our responses and adaptations are adequate to accept this manuscript for publication in Biogeosciences. Please find our detailed responses below.**

#### **Anonymous Referee #1**

Received and published: 17 February 2015

The manuscript by Steeb et al. consists of two parts. One explores the current in situ methane geochemistry at two sites in the Quepos Slide (offshore Costa Rica) whilst the other uses sediments from these sites to simulate the effects of changing fluid flow conditions on the sedimentary biogeochemistry using a flow through reactor. The first part concludes that the benthic filter at these sites is highly efficient, with AOM serving as an effective barrier for methane seepage into the water column. Seepage velocities are also extracted from the numerical model. The second part concludes that, under the conditions of the flow-through experiment, the benthic filter can cope with a wide range of fluid flows (0.5-5 microL/min delivering 0.28-2.8 mmol m<sup>-2</sup> d<sup>-1</sup> methane, respectively) for up to 316 days, with a change in the flow regime at 260 days. The paper is well written and contains interesting insights. I think, however, that the manuscript could benefit from additional discussions and more emphasis on the assumptions behind both the numerical model and the experimental setup. The following summarizes some criticisms of specific sections:

#### Introduction:

The introduction centered mainly on seeps and AOM, but only tangentially discusses the scientific question or the aims that the manuscript wants to address/ achieve. Background information is good and important, but it is not until the last sentence in the introduction that the authors tacitly frame their research question. Further information that should go either in the introduction or in the Methods section should be the reason for the given approaches and how these approaches complement each other.

**Authors Reply:** We would like to thank the reviewer for this helpful comment. We restructured and edited the last section of the introduction to provide a better overview of our goals and applied methods.

#### Numerical Model:

The modelling exercise was performed in order to determine the site-specific areal AOM rates and fluid velocities. In general the model parameters are highly unconstrained, for example, what determines the lower boundary of the model?

(i.e. What evidence exists for hydrates at 50-80 cmbsf?).

**Authors Reply:** We found no evidences for gas hydrates, such as visible hydrates or porewater dilution, in the multicorer cores (44 cm length), which was not surprising as the study site was above the gas hydrate stability zone. We used the equations by Tishenko et al. 2005 to calculate the sediment methane concentration at the lower boundary.

Table 4 shows over 13 parameters are fitted, what procedure was used to determine a best fit?

Some of the fitted values seem exceptional and would thus require additional justification (i.e. 80 yr<sup>-1</sup> non local mixing). Is the entire core length the mixing depth?)

**Authors Reply:** The reviewer asserts that the model is highly unconstrained. The model (like all models) simplifies the biogeochemistry and physics of natural settings. However, at seeps, the major biogeochemical processes occurring in surface sediments are limited to sulfate reduction, AOM, and precipitation of sulfide. The measured geochemical profiles contain all the information (diffusive gradients etc.) needed to constrain these rates and parameterizations quite well, as well as the upward fluid flow velocities. We did not use an optimization procedure to parameterize the model since the modeled profiles are quite sensitive to the parameters given in Table 4 (now Table 2). In other words, the entire set of data allows the parameters to be well constrained. Yet, the burial velocity is more unconstrained than other parameters. This is not of major concern at our site because the solute transport is dominated by fluid advection and non-local transport. The lower boundary conditions of the model (fixed concentrations) are simply determined from the measured data. (The non-local transport of 80 yr<sup>-1</sup> is a maximum value at the sediment surface, which attenuates toward zero at 2 cm depth).

What evidence exists for steady state conditions?

**Authors Reply:** This is a necessary assumption to derive the background rates of AOM. We acknowledge the possibility that the geochemical profiles are not in steady state. We have no temporal data to investigate this further.

In the rate-fitting simulations, only AOM was taken into account while SRR was ignored. Justification for these assumptions and further clarifications are required in order to correctly interpret the results of the numerical model.

**Authors Reply:** As our model did not consider organoclastic sulfate reduction, sulfate reduction rates equaled AOM rates. We therefore refrained from showing the modeled sulfate reduction, as now new information would be gained.

SLOT experiment:

Maybe I missed it, but the dimensions of the SLOT cores should be given. I can infer them from the porosity data and the pore water residence time, but this does not allow for an independent assessment of the residence time. Consequently, it is also difficult to tell how much pore water was removed during the extractions with respect to the total volume of pore water. This is important to determine how the pore water concentrations may shift during the rhizon extractions. It would also help to establish to what extent the SBTZ movement is due to AOM vs. fluid displacement.

**Author Reply:** Diameter of the SLOT liners (6 cm) was added (see 2.5). The exact technical drawings of the liners can be found in Steeb et al 2014. With the normal rhizon sampling procedure, 8.1 % of porewater is removed from each sampling layer. This porewater is replaced by porewater from adjacent layers and ultimately by the seawater medium in the supernatant. This 8.1% replacement/dilution plus an analytical precision of <1% (ion chromatography) and 0.1% (TA titration) adds up to a total analytical error of ca. 9% and 8.2% for sulfate/bromide and TA, respectively. We added this information to 2.6. Sulfide, pH, and redox potential were determined prior to porewater sampling (with microsensors) and are therefore likely not affected by the rhizon sampling.

A great deal of the discussion focuses on comparing the flux and AOM results of the SLOT experiment with those at other nearby sites. As the methane flux cannot be replicated due to pressure constraints, perhaps the authors could collect methane flux (both from the source and out of the sediment), AOM, fluid flow, and other environmental information from various seeps into a table to facilitate the comparison, especially as these results are at odds with the modelling and field observation of Karaca et al. (2012) and Bohrmann et al. (2002).

**Author Reply:** We thank the reviewer for this suggestion. We added an overview of fluid flow rates, benthic methane emissions, methane fluxes, and ex situ rates of AOM in comparison with previous studies at cold seep sites covered with sulfur bacteria mats. See new Table 5. We hope this overview puts our data into a better perspective.

It appears to me, based on the information provided in the manuscript, that the limitations of the experiment would make it impossible to extrapolate the results to field conditions, especially since at seeps sites methane is often found to bypass the anaerobic zone and supply energy for many aerobic communities (Boetius and Wenzhöfer, Nature Geoscience, 6, 725–734, 2013). I thus feel that better context of the experiment, such as the different methane to sulfate ratios possible in the SLOT experiment in comparison to field sites, warrants further scrutiny.

**Author Reply:** We are well aware of the limitations of the SLOT system, which have been broadly discussed in the original publication of this method (Steeb et al. 2014). The main reason for applying this method is to study the response of AOM and the SMTZ to different fluid flow regimes. But the reviewer is right that we should emphasize this point stronger in the present publication. We therefore highlighted the methodological limitations of the SLOT system in the method part (2.5).

Minor revisions:

Page 16037 line 9 Parenthesis missing.

**Author Reply:** Sorry, we did not find a parenthesis missing in this line.

Page 16039 line 15 remove “by”.

**Author Reply:** Done

## Anonymous Referee #2

Received and published: 16 March 2015

I found this manuscript a very interesting approach to investigate the adaptation of the anaerobic benthic methane filter to changing fluid flow. The authors use the common methods to derive key parameters of methane consumption in surface sediments. Then they use sub-cores for an experiment in the laboratory. They found that the zone of AOM decreases with increasing fluid flow and that most of the methane is consumed when methane flux is below 3 mmol m<sup>-2</sup> d<sup>-1</sup>. Only rapid changes cause an increase in methane efflux. Although I like the approach, I found that more details in the method part and a clearer discussion would greatly improve the manuscript.

Major concerns:

1. The variability in the porewater chemistry appears not coherent with a steady state situation. Fig. 3 and 4 illustrate that not only sulfide as described, but also the other analyzed parameters vary over time, only the establishment of a SMTZ in the high flow experiment appears stable.

**Author Reply:** During most of the incubation time, the cores were not in steady-state. The system started with zero fluid flow to which then a low or high fluid flow was applied. It was the purpose of this study to follow the response of biogeochemical parameters to these applied flows. Towards the end of the incubation, a quasi steady state situation was reached in the high flow core, as we did not observe any more pronounced changes in the profiles. Steady state was never reached in the low flow core (see also additions to 4.1).

It would be helpful to know the precision of the measurements and how much water was taken from the experiment for the different analyses. Could you also indicate what changes in the concentrations can be expected if xx ml porewater are withdrawn from the experiment. After gaining an understanding of the typical errors due to porewater withdrawal and analytic procedures, one would know what are the 'real' changes over time and if a near steady state situation was reached.

**Author Reply:** With the normal rhizon sampling procedure, 8.1 % of porewater is removed from each sampling layer. This porewater is replaced by porewater from adjacent layers and ultimately by the seawater medium in the supernatant. This 8.1% replacement/dilution plus an analytical precision of <1% (ion chromatography) and 0.1% (TA titration) adds up to a total analytical error of ca. 9% and 8.2% for sulfate/bromide and TA, respectively. We added this information to 2.6. Sulfide, pH, and redox potential were determined prior to porewater sampling (with microsensors) and are therefore likely not affected by the rhizon sampling.

The low methane flux in the experimental setup (page 16055, line27 et seq.) raises the question, why was not more methane pumped into the system. Was there a reason for choosing a 1mM concentration for the methane-rich solution? Could you please calculate the methane solubility in situ in contrast to your experiment and use the value to explain the low methane flux. What maximum methane solubility would have been possible to achieve in your experimental setup?

**Author Reply:** The SLOT system operated at atmospheric pressure (1.07 bar). The solubility of methane at the experimental pressure, temperature (10° C) and salinity (35 PSU) is around 1.5 mmol l<sup>-1</sup>, calculated after Yamamoto et al. 1976. Unfortunately we were not able to achieve this theoretical concentration, for reasons unknown (see extensive discussion in the original method publication by Steeb et al. 2014). The highest and relatively stable methane concentration we archived was around 1 mmol l<sup>-1</sup> (965±180 µmol l<sup>-1</sup>). We highlighted the system's limitations in the method part (2.5) and referred to Steeb et al. 2014 for more details on the advantages and disadvantages of the method. We hope this information is sufficient, as we would like to avoid to repeat this discussion.

2. The different efficiencies of AOM (page 16056, line 19 et seq.) could also be due to different transport processes in the experimental setup in contrast to the natural environment. In the experiment the solutes are transported by diffusion, but in the natural environment fractures of different sizes might play a more dominant role (Mau et al., 2006). This thought is missing in the discussion and could be included.

**Author Reply:** In the experiments, the solutes were not transported by diffusion but by advection (fluid flow). But the reviewer is absolutely right that fractures in the core can enable faster transport. We observed such a possible transport mechanism in the low flow core (bromide and methane in the outflow) and discussed it (see 4.1)

3. From the conducted experiment one can state that methane ascending at a rate of up to  $3 \text{ mmol m}^{-2} \text{ d}^{-1}$  is completely consumed by AOM. Is this coherent with published data? It would be nice if a table with methane fluxes and AOM-rates that are mentioned throughout the manuscript would provide a quick overview of what values were measured, modeled and how the experimental derived data fits to those.

**Author Reply:** We appreciate this suggestion and added an overview of fluid flow rates, benthic methane emissions, methane fluxes, and ex situ rates of AOM in comparison with previous studies at cold seep sites covered with sulfur bacteria mats. See new Table 5. We hope this overview puts our data into a better perspective. The areal rates of methane oxidation at seep sites vary over a broad range. At hot spots like Hydrate Ridge (Treude et al. 2003) or Mound 11 (Krause et al. 2014) AOM rates of more than  $100 \text{ mmol m}^{-2} \text{ d}^{-1}$  were observed.

4. It should be clearly indicated that only one value for the response time was derived from the experiment and that further studies need to validate this value. Also, on page 16058, line 6, you write 171 days whereas on page 16060, line 8 you provide a range 150-170 days. Please clarify this contradiction.

**Author Reply:** After 171 days no further methane decrease was detected in the HFC, therefore no further change in the efficiency of AOM was expected. However, final efficiency might have established at an earlier time point (between the 105 and 171d measurement). From the fit of methane concentrations in the outflow, we estimated a response time between 150 and 171 days. But the reviewer is right, we do not actually know what happens between measurements and therefore changed the response time in the conclusion to ca. 170 d. We also highlighted that more measurements are required to validate our results.

5. The method section needs more details. At what temperature were the cores for the experiments transported from the cruise to the lab?

**Author Reply:** The sediment cores were transported at  $4^{\circ}\text{C}$  and stored at  $0^{\circ}\text{C}$ . Information added to 2.5

At what temperature was the experiment performed?

**Author Reply:** The experiments were performed at  $10^{\circ}\text{C}$ . Information added to 2.5

These temperatures should be included in the manuscript as the temperature influences the solubility of methane.

Why were both media, also the resembling seawater media kept anoxic? There is still sufficient  $\text{O}_2$  in the water although located in the OMZ (page 16041, line 23). Is it because you liked to focus on the anaerobic methane consumption, then it should be clearly stated.

**Author Reply:** Yes, we focused only on AOM, as it is the most important process for removing methane from the sediment. We added this information to 2.5. But more importantly, oxic conditions in the overlying water would have compromised our methane budgeting, as we would not have been able to exclude aerobic methane oxidation in the supernatant, which could be powerful when kept in containment without dilution through currents. Furthermore, adjusting the seawater medium in the system to a constant (in situ) concentration of  $6 \mu\text{mol l}^{-1}$  for over one year would have been a completely new challenge.

6. Tables and figures:  
The order of the tables in the text is not consecutive (Table 1, Table 4, and then Table 2).  
Table 3 is not mentioned in the text.

**Author Reply:** Thank you for noticing. We corrected/added all Table citations.

Fig. 5 is missing in the text, but should be included on page 16051, line 14 and 26.

**Author Reply:** Thank you for noticing. We added the citation to 3.2.2

Figure references in text include supplements, e.g., Fig. 3a-u, but these supplements are not shown in the figures.

**Author Reply:** Unfortunately, we are not sure what the reviewer meant. Fig. 3 has supplements from a-u.

It would be better to use the same scale for sulfide in all plots of Fig. 3 and 4 (possibly log-plots are better?) otherwise mention it in the figure caption that sulfide concentrations are plotted on different scales.

**Author Reply:** We agree that one scale for one chemical species is usually better. Unfortunately with the same scale it would not be possible to see sulfide values at the lower concentration range. A log scale is also not possible as many concentrations are zero. We would therefore like to keep the scale as is.

The supplements of Fig. 5, e.g., Fig. 5 a and b, do not match with the figure itself. Methane concentration in the outflow is shown in A and D, but not in A and B.

**Author Reply:** Thank you for noticing. We changed the supplement ID accordingly.

7. Minor changes:  
Some references are not in brackets, page 16037, line 8, page 16038, line 24, page 16040, line 22.

**Author Reply:** The brackets were actually in the submitted manuscript. They must have been lost when the discussion paper was produced.

Delete 'huge' on page 16037, line 12.

**Author Reply:** Done

Add year of sampling in method section

**Author Reply:** Done

Change 'controls samples' to 'control samples' page 16040, line 13

**Author Reply:** Done

Change 'several month' to 'several months' page 16040, line 24

**Author Reply:** Done

The sentence: 'Further details on the SLOT sampling procedure..' page 16045, line 14, can be deleted as it was mentioned before.

**Author Reply:** This citation refers only to the sampling procedure and should remain here.

I found it confusing to talk about a moderate flow rate but call the experiment low flow, page 16042, line 3-5.

**Author Reply:** Its true that it sounds strange within the broader perspective, but compared to the high flow setup it was a low flow.

I suggest to delete 'than expected' on page 16056, line 16, as it otherwise sounds as if you did not know how much methane was pumped into your experimental system.

**Author Reply:** We deleted "expected"

Rephrase sentences on page 16057, line 16 to 'We assume that at most 80% of the sulfate reduction . . . can be related to.. Most likely, this ratio is less, because ex situ radiotracer incubations. . .'. In addition, I suggest to rewrite the last sentence of the paragraph page 16057, line 20 to clarify that the organic matter degradation is higher near the seafloor and decreasing with sediment depth.

**Author Reply:** Done

### **Anonymous Referee #3**

Received and published: 17 March 2015

In this manuscript, the authors first measure anaerobic methane oxidation in sediments at the Quepos Slide site, and then conduct laboratory experiments to study how anaerobic methane oxidation changes in response to changes in fluid flow. I find this approach quite interesting, and it addresses important questions about how sediment microbes adjust to changing methane fluxes. I appreciate the technical difficulties with setting up these types of experiments with intact sediment cores, and while the approach here may not have perfectly replicated field conditions (lower methane concentrations, lack of oxic surface sediment, pore water removal for sampling, etc.), it's an excellent start. I agree with the other reviewers that it would be helpful to better describe the issue of pore water removal during the experiment, but otherwise I feel that the authors have sufficiently addressed the methodological issues.

Other minor issues:

Page 16036, line 1-2: is it 160 m or many hundreds of m?

**Author Reply:** Changed to several hundreds of meters

Page 16039, line 20-24: what size vial? And I assume the GC had a FID?

**Author Reply:** Information (30 mL, FID) was added to 2.2

Page 16059, line 20: slow or abrupt, which one?

**Author Reply:** You are right, it must be abrupt, since the changes in our system are immediate.

Figures 3 and 4: These are pretty hard to read. A bit more space between the panels would help make it easier to tell what's being plotted in which figure. It might also help if the two shapes were more distinct. Until I zoom way in, the circles and diamonds are hard to distinguish.

**Author Reply:** We are sorry, but we can't technically accommodate this request at the moment.

Figure 5: I think the subpanel labels don't properly match the caption

**Author Reply:** We corrected the labels.

**P. R. Dando**

pdando@mba.ac.uk

Received and published: 13 January 2015

General comments

This paper describes experiments, using 16 cm long sediment cores, to examine how the microbial community in sediments from a cold seep off Costa Rica respond to changes in seepage flow. In particular, how the rate of anaerobic oxidation of methane changes over time. A synthetic, methane-rich, seepage solution was pumped into the core base and sulphate was allowed to diffuse into the core from the surface, to simulate natural conditions. Samples were withdrawn from the cores at approximately 1 cm depth intervals and at periods during the experiment. The experiment showed clear geochemical changes in the cores over time and demonstrated that the microbial rates adjusted, with time, to increased or decreased flows.

A detailed critique of the experiment is given below.

This paper would be enhanced by a section looking at the advantages and disadvantages of the technique and discussing alternative approaches.

**Author Reply:** A full discussion of the advantages and disadvantages of the SLOT system is provided in the original publication of this method (Steeb et al. 2014, *Limnology & Oceanography Methods*).

1. One problem with the experimental technique was that, even after 258 days, the system had not reached equilibrium, partly due to the long residence time of the pumped fluid.

**Author Reply:** We are aware of this issue. While the HFC reached quasi steady-state conditions, the LFC was still in the transition phase. You might argue if true steady state (or equilibrium) is ever reached in natural advective systems or if this is more of a theoretical concept. But that would be a different discussion. For our study, this is as good as it could get, since experimental runtimes of over 1 year are difficult to maintain. We already discussed the fact that steady state was probably not reached in the LFC (see 4.1) and added some more comments about it into section 4.2.

2. In addition, the method and frequency of sampling may have affected the rates. The least invasive technique to study changes in a flow through system would be to measure just the inflow and outflow.

**Author Reply:** Well...yes and no. If you just measure the in and outflow, which we fully agree would be the most non-invasive method, you have a black box and would learn nothing about the evolution of geochemical gradients and the position of the SMTZ. Such systems have been created before (see, e.g., publications by Girguis or Wegener et al.) but they aimed at different research questions. For our purpose, this system was the best compromise. For a detailed comparison between the SLOT system and other systems, please refer to Steep et al. 2014.

The authors could discuss whether using short (syringe) cores, with sediment taken from the SMTZ and from above and below this zone, in a flow system might be more effective. Equilibrium should be reached more quickly and it would be simple to study how the microbial community at different depths responded.

**Author Reply:** We thank the reviewer for his comment, but will not discuss this aspect, because it is not the purpose of this paper to repeat the method discussion. Please refer to Steeb et al. 2014 for all the details. It would also not be advantageous to pick sediments from different depths and study them in short cores, as it would not be normal for deep sediments section to have such a short (diffusional) distance to the overlying, sulfate-rich water. This application would create even more artifacts.

A disadvantage of this is that it would not allow for the migration of bacteria in the seep fluid from deeper to shallower layers.

SLOT-System:

3. Subsampling the MUC core samples with the SLOT core tubes, if done by just pushing the latter into the former, as described in Steeb et al. (2014), given the core tube thickness, would cause sediment compression. There is no mention of the degree of compression caused, i.e. how much lower the sediment surface was in the SLOT tube compared with the MUC tube. The way to overcome this is to either use a piston, that is withdrawn at the same rate as the core tube is advanced, or by using a controlled vacuum applied to the top of the core to keep sediment levels equal as the tube is pushed deeper.

**Author Reply:** We tried sub-sampling with the SLOT liner (6 cm diameter) using a piston similar to what is done for the small rate liners (2.6 cm diameter), but given its much larger diameter, it was

difficult to apply the right vacuum. In the end it worked pretty well by just slowly pushing the SLOT liner into the MUC core. The sediment level inside the SLOT liner remained on the same level as the MUC sediment level. No sediment compaction was obvious, although it might not have been completely avoided. Keep in mind that the piston method has its own flaws. If the applied vacuum is stronger compared to the speed at which the liners are pushed into the sediment, the sediment is sucked above the MUC core sediment level, which will also affect sediment properties.

4. Sediment would be further consolidated by the downwards pumping of water through the core during the 40 day "preparation phase". The pumping rate used during this phase is not stated. Thus the density of the sediment in the experimental cores may not reflect that of the sediment in situ. Both SLOT cores had a lower porosity than the MUC core (Figs. 8 & 9), suggesting sediment compression.

**Author Reply:** We added the pump rate (thanks for noticing), which was 20 ul/min, and added a comment about potential sediment compaction to the method (see 2.5).

5. The volume of pore water removed during the sampling periods appears to be excessive and may have had an effect on the experiment. Assuming that the core i.d is 6 cm (Steeb et al 2014), the core length is 16 cm and porosity is 0.85, then each core contains approximately 385 ml of pore water. With 16 sediment sampling points per core (Fig. 3) and 1.5-2ml/sample, then 24-32 ml of pore water is removed every sampling period, i.e 8 % of the pore water volume in the core. This would have to be replaced either by sediment compaction or by advection from the surface and I do not see how it can be stated "sulfate was transported into the sediment core solely via diffusion". Thus, for the low-flow experiment, advection from the surface to replace the pore water sampled, would be almost equivalent to the flow from the core base over the period to the 49 day sampling interval. This would have the effect of displacing the SMTZ downwards. In the high flow experiment the effect of removing pore water by sampling is reduced since the advective flow due to the pumped "seep water" would be much greater than the downward advection due to pore water removal.

**Author Reply:** The reviewer is absolutely right. The removal of porewater with rhizons is causing a smoothening of the geochemical profiles. This effect has been thoroughly discussed in the original publication of the method (Steeb et al. 2014). We added this information to the methods (see 2.5)

6. The bromine profiles in the low flow experiment are not adequately explained. It would help to visualize what happened by altering the scale of the bromide concentrations in Fig. 3. Why was Br elevated in the overlying water after 105 days but this disappeared subsequently? Could there be channels that opened and closed over time?

**Author Reply:** It is possible that a sudden channeling caused a spontaneous emission of advective water into the supernatant and then disappeared again. We can only speculate. We noted the increase of bromide in the supernatant in the results (see 3.2.1) and further highlighted channeling in the discussion (see 4.1).

7. The authors note that the "methane concentrations were lower than those potentially encountered under in situ conditions because the cores were not pressurized". Certainly some of the concentrations measured in core S0206-31 would lead to over-saturation at atmospheric pressure and bubble formation when the core was recovered. We are not told whether this occurred and gas channels could have formed in the SLOT cores, leading to channeled advection of the pumped "seep water".

**Author Reply:** Small bubbles formed after core retrieval (noticeable as "foamy" sediment) but no bubble release at the surface was visible. The bubbles disappeared after a while, probably through a combination of consumption, dissolution and diffusion. We can only speculate about channels formed through gas bubble formation. It is likely that the permeability of the sediment increased while foamy and decreased again after bubbles disappeared. Since the cores were not immediately set up in the SLOT system, but first stored on board and then transported to Germany (total ca. 170 days, information added to 2.5), there was plenty of time for the sediment to resettle.

It would also be interesting to know what effect the insertion of the line of rhizomes has on flow dynamics in the cores.

**Author Reply:** Of course the rhizons had some effect on the flow dynamics, but since the effect was the same for the high and the low flow core, we are confident that we can compare. We noticed that the sediment showed basically no resistance when the rhizons were introduced, which would suggest

that the sediment was able to easily settle around them. But keep in mind that seep sediments are naturally heterogeneous. We like to compare it with crunchy peanut butter, due to the presence of carbonate pebbles. Plus sometimes clamshells are buried in the sediment. Seep sediments are complex and we can only try to mimic reality but will never fully reach it.

AOM rates cannot be accurately calculated in the LFC core by using differences in the methane inflow and outflow concentrations at 258 days. Firstly, equilibrium has not been reached at this time, only 186 ml of “seep water” had been delivered to the core at this time.

**Author Reply:** This is correct. We added a note to the results (see 3.2.1 and 3.2.2) and discussion (4.1 and 4.2) and also highlighted in the new Table 5 that AOM rates from the LFC/NHFC are most likely overestimated.

Secondly no rates of methanogenesis within the core were measured and since the outflow contained 0.9  $\mu\text{M}$  at this stage, in an anoxic core full of sulphate, it implies possible methane generation within the core or channeling.

**Author Reply:** We do not understand, why a core full of sulfate implies methanogenesis, as the presence of sulfate, i.e. sulfate reduction, usually excludes methanogenesis unless it is based on non-competitive substrates (e.g. not used by sulfate reducers). We cannot exclude non-competitive methanogenesis, but the methane production was probably minor compared to the methane supplied by the medium. We would assume that the established AOM community quickly removed the produced methane. We think that channeling is a more likely explanation for methane in the outflow of the LFC.

Without information on how much methane-free water was pumped through the core during the initial 40-day period it is not possible to assess how much methane might have been left in the core.

**Author Reply:** See information above. It is unlikely that any residual methane remained in the core during the ca. 170 days of storage and transport. The active AOM community most likely consumed all methane before the core was set up in the SLOT System.

It would have been helpful had the authors measured methane directly at each sampling period, since this can be done on sample volumes as small as 50 $\mu\text{l}$ , either by direct injection of pore water (as sometimes used for pore water bicarbonate) or by using small headspace vials.

**Author Reply:** We are not sure if we understand this suggestion. Does the reviewer suggest determining methane from rhizon samples? Rhizon sampling is not recommended for volatile substances, as vacuum is applied.

8. Hydrological residence time No units were given for this and I was unable to follow the calculation, “the average time of the seepage medium to flow through the sediment column and was calculated by dividing the pore water volume by the flow rate”. For the low flow system, with an approximate pore volume of 390 ml and a flow of 0.5  $\mu\text{l min}^{-1}$ , the HRT should be 541 days. How was the figure of 1080 derived?
9. **Author Reply:** The reviewer is right and wrong. It is correct that 1080 d is not the time the seepage medium needs to pass the core, but to pass from inflow to outflow (which was used to calculate areal rates, see Table 4). The residence of the medium to pass the core must take into account the volume below the core (between inflow and core) and the sediment porewater volume, which amounts to a residence time of 696 d for the LFC and 69 d for the NHFC. We corrected accordingly (see 2.5 and 4.1).

Text queries and corrections

Abstract

“Most of the dissolved methane reaching the seafloor at cold seeps is oxidized within the benthic microbial methane filter by anaerobic oxidation of methane (AOM).” Surely the methane reaching the seafloor has already passed the benthic AOM, since this is below the seafloor.

**Author Reply:** We rephrased.

Introduction

“methane gas may be transported upwards in solution by molecular diffusion or by ascending fluids mobilized by - - - (ii) formation of gas hydrates within the gas hydrates stability zone”. How does hydrate formation aid upward transport of methane?

**Author Reply:** We rephrased.

#### Methods

The detector used for determining methane is not mentioned

**Author Reply:** FID, we added information to 2.2 for the field measurements. Analytical methods for the SLOT cores were identical to Steeb et al. 2014.

and it is not made clear how the concentrations are calculated, are they per liter of sediment or pore water?

**Author Reply:** We added information (for all parameters) to the figure captions. It was per sediment for the field data and per porewater for the SLOT experiment.

One would assume the latter but there is no mention of porosity measurements in the methods, other than for the SLOT cores. The use of mM, rather than mmol l<sup>-1</sup>, would have clarified this.

The incubation temperature for the SLOT cores is not given and we do not know how this differed from the in situ temperature (or how constant temperatures are in Slide sediments).

**Author Reply:** We added information to 2.5. The incubation temperature was 10°C, the in situ temperature was 8°C.

Section 2.7 "At the end of the experiment, 1.5mL porewater from each depth was sampled for determinations of sulfide (0.5 mL), sulfate and bromide (1.0 mL) as well as total alkalinity (0.5 mL)," These individual volumes add to 2.0 ml, not 1.5.

**Author Reply:** Thanks for noticing. We actually took only 0.5 mL for sulfate and bromide (IC). We changed accordingly.

#### Results

In section 3.2.3 it is stated that the experiment was terminated "after 350 day runtime" although runtime in Figures 3, 4 and elsewhere is calculated from the end of the 40 day initial period.

**Author Reply:** That is correct, all runtimes are given after the 40 days initial period. Hence, the total runtime is 350 days (not 390 days).

# 1 Efficiency and adaptability of the benthic methane filter at Quepos Slide cold 2 seeps, offshore Costa Rica

3 Philip Steeb<sup>1\*</sup>, Stefan Krause<sup>1</sup>, Peter Linke<sup>1</sup>, Christian Hensen<sup>1</sup>, Andrew W. Dale<sup>1</sup>, Marianne Nuzzo<sup>2</sup>,

4 Tina Treude<sup>1,3\*</sup>

5 <sup>1</sup>GEOMAR Helmholtz Centre for Ocean Research Kiel, Wischhofstrasse 1-3, D- 24148 Kiel, Germany

6 <sup>2</sup>LNEG, Marine Geology Department, Alfragide, Portugal & Institute Dom Luiz, University of Lisbon,  
7 Lisbon, Portugal. Now at Integrated Geochemical Interpretation, Ltd. (UK)

8 <sup>3</sup>Present address: [University of California, Los Angeles, Department of Earth Planetary & Space](#)

9 [Sciences and Department of Atmospheric and Oceanic Sciences, Los Angeles, CA, USA](#)

10 \*Corresponding Authors: [psteeb@geomar.de](mailto:psteeb@geomar.de), [ttreude@g.ucla.edu](mailto:ttreude@g.ucla.edu)

11 Working Title: Quepos Slide SLOT System

## 12 Abstract:

13 Large amounts of methane are delivered by fluids through the erosive forearc of the convergent  
14 margin offshore Costa Rica and lead to the formation of cold seeps at the sediment surface. Besides  
15 mud extrusion, numerous cold seeps are created by landslides induced by seamount subduction or

16 fluid migration along major faults. Most of the dissolved methane [migrating through the sediments](#)

17 [of](#) cold seeps is oxidized within the benthic microbial methane filter by anaerobic oxidation of

18 methane (AOM). Measurements of AOM and sulfate reduction as well as numerical modeling of

19 porewater profiles revealed a highly active and efficient benthic methane filter at Quepos Slide site; a

20 landslide on the continental slope between the Nicoya and Osa Peninsula. Integrated areal rates of

21 AOM ranged from  $12.9 \pm 6.0$  to  $45.2 \pm 11.5$  mmol m<sup>-2</sup> d<sup>-1</sup>, with only 1 to 2.5% of the upward methane

22 flux being released into the water column.

23 Additionally, two parallel sediment cores from Quepos Slide were used for in vitro experiments in a

24 recently developed Sediment-Flow-Through (SLOT) system to simulate an increased fluid and

25 methane flux from the bottom of the sediment core. The benthic methane filter revealed a high

26 adaptability whereby the methane oxidation efficiency responded to the increased fluid flow within

1

Tina Treude 13.8.2015 15:51

**Gelöscht:** [ttreude@geomar.de](mailto:ttreude@geomar.de)

Tina Treude 12.8.2015 19:43

**Gelöscht:** reaching the seafloor

Tina Treude 12.8.2015 19:43

**Gelöscht:** at

ca. 170 d. To our knowledge, this study provides the first estimation of the natural biogeochemical response of seep sediments to changes in fluid flow.

## 1. Introduction:

Subduction zones represent large-scale systems of sediment and element recycling. Organic carbon accumulation at continental margins can lead to the formation of large methane reservoirs through its biological or thermogenic breakdown (Judd et al. 2002; Schmidt et al. 2005; Hensen and Wallmann 2005; Crutchley et al. 2014). Produced methane gas may be transported upwards in

solution by molecular diffusion or by ascending fluids, mobilized by, e.g., sediment compaction or clay mineral dehydration (Hensen et al. 2004; Tryon et al. 2010; Crutchley et al. 2014). When the fluids are highly enriched in hydrocarbon gases, gas hydrates may precipitate depending on the pressure-temperature conditions (Hensen and Wallmann 2005). Gas hydrates sometimes block fluid pathways (Tryon et al. 2002; Minami et al. 2012) and change the composition of fluids flowing through the gas hydrate stability zone (GHSZ). Alternatively, dissociating gas hydrates can act as additional sources for methane and fluids (Kvenvolden 2002), or dilute fluids when they dissolve (Hesse et al. 2000; Hensen et al. 2004).

The migration of methane-charged fluids towards the sediment-water interface creates so called "cold seeps" (Judd et al. 2002; Suess 2010). Within the surface sediment, the majority of the methane is consumed by the anaerobic oxidation of methane (AOM) (Hinrichs and Boetius 2002; Knittel and Boetius 2009). AOM is coupled to sulfate reduction and produces dissolved bicarbonate and sulfide. The reaction is mediated by a consortia of anaerobic methanotrophic (ANME) archaea and sulfate-reducing bacteria (SRB) (Boetius et al. 2000). Recent studies propose that some ANME can reduce sulfate without the aid of SRB (Milucka et al. 2012). Additionally, the use of other electron acceptors such as Mn, Fe (Beal et al. 2009), or nitrate (Ettwig et al. 2010) is also possible. However, sulfate is the most abundant electron acceptor in seawater and AOM coupled to sulfate reduction is,

Tina Treude 13.8.2015 15:52

Gelöscht: 150-

Tina Treude 11.8.2015 13:35

Gelöscht:

Tina Treude 11.8.2015 13:28

Gelöscht: (i)

Tina Treude 11.8.2015 13:35

Gelöscht: and (ii) formation of gas hydrates within the gas hydrates stability zone (GHSZ) (Torres et al. 2004; Burwicz et al. 2011; Wallmann et al. 2012)

63 to our knowledge, the by far most important anaerobic pathway for methane oxidation in marine  
64 settings (Reeburgh 2007).

65 The sediment zone, in which methane and sulfate concentrations overlap, is termed the sulfate-  
66 methane transition zone (SMTZ). The depth of the SMTZ is dependent on (1) sulfate depletion  
67 resulting from organic matter degradation (Borowski et al. 1999), (2) sulfate supply by diffusion,  
68 bioirrigation and sulfide re-oxidation reactions (Dale et al. 2009), (3) the flux of methane from below  
69 the SMTZ (Borowski et al. 1996), and (4) the advective fluid flow rate (Treude et al. 2003; Orcutt et al.  
70 2011). At continental margins, the SMTZ can sometimes be located several hundreds of meters  
71 below the seafloor (mbsf) (Borowski et al. 1999). In coastal sediments, sulfate is consumed rapidly via  
72 organoclastic sulfate reduction fueled by an enhanced supply of organic matter and, subsequently,  
73 the SMTZ is often located closer to the sediment-water interface compared to sediments in greater  
74 water depths (Hinrichs and Boetius 2002). At seepage sites, upwards advective flow of methane-rich  
75 fluid pushes the SMTZ closer to the surface, occasionally to only a few centimeters below the  
76 seafloor (cmbsf) (Treude et al. 2003; Niemann et al. 2006; Krause et al. 2014). At the center of the  
77 Håkon Mosby Mud Volcano, advective fluid flow is so high that it inhibits sulfate penetration into the  
78 sediment (de Beer et al. 2006; Niemann et al. 2006), resulting in the absence of a SMTZ. The depth of  
79 the SMTZ determines, which chemolithotrophic seep organisms have access to the produced sulfide.  
80 The prevailing communities serve as indicators of seepage intensity. Sites covered by mats of sulfur  
81 bacteria (e.g. *Beggiatoa*) exhibit a very shallow SMTZ (few cm) compared to clam sites (e.g.  
82 *Calyptragenia*) with SMTZ depth of ~5-10 cm, or even deeper SMTZ in tubeworm or *Solemya* habitats  
83 (Sahling et al. 2002; Levin 2003; Treude et al. 2003; Mau et al. 2006; Fischer et al. 2012).

84 In the present study, we compared data from field measurements, numerical modeling, and  
85 laboratory flow-through experiments of samples taken at Quepos Slide, a submarine landslide on the  
86 Pacific coast off Costa Rica (Bohrmann et al. 2002; Karaca et al. 2012), to investigate the effect of  
87 fluid flow on methane consumption and emission. The numerical model was developed to compare  
88 with direct measurements of AOM and sulfate reduction rates and to determine the magnitude of

Tina Treude 11.8.2015 13:38

**Gelöscht:** T

Tina Treude 11.8.2015 13:38

**Gelöscht:** be located as deep as 160

Tina Treude 11.8.2015 13:38

**Gelöscht:** at continental margins and sometimes even many hundreds of meters deep

Tina Treude 11.8.2015 13:44

**Gelöscht:** this

Tina Treude 11.8.2015 13:48

**Gelöscht:** present the first direct rate measurements of AOM and sulfate reduction for

Tina Treude 11.8.2015 13:48

**Gelöscht:** .

Tina Treude 11.8.2015 13:50

**Gelöscht:** A

Tina Treude 11.8.2015 13:50

**Gelöscht:** the rate

102 the fluid advection velocity. In laboratory experiments, undisturbed sediments from Quepos Slide  
103 were exposed to different flow conditions, to investigate the development of the SMTZ and the  
104 response of the benthic microbial methane filter. For this objective, we used a newly developed  
105 Sediment-Flow-Through system, referred to as SLOT (Steeb et al. 2014), which mimics natural fluid-  
106 flow regimes. It was the overall goal of this study to better understand mechanisms controlling the  
107 efficiency of this methane filter, which plays a major role in reducing greenhouse gas emissions from  
108 the ocean into the atmosphere (Reeburgh 2007).

110 **1.2 Geological Setting:** At the Mid-American Trench, the Cocos Plate in the north and Nazca Plate in  
111 the south are subducted below the Caribbean Plate at a velocity of 8.8 cm yr<sup>-1</sup> (Syracuse and Abers  
112 2006). Here, seep features like mud volcanoes, mud diapirs, and pockmarks are very abundant. More  
113 than 100 seeps localities have been identified at the central Costa Rican Pacific Trench, on average  
114 one seep every 4 km (Sahling et al. 2008). Recent high-resolution mapping revealed even greater  
115 seep density in this region (Kluesner et al. 2013). Between the Nicoya (north) and Osa Peninsula  
116 (south), seamounts from the Nazca Plate are subducted (Ranero and von Huene 2000), resulting in  
117 slope failures and landslides or scarps (e. g., Jaco Scarp, BGR landslide, GEOMAR landslide; Harders et  
118 al. 2011; Ranero et al. 2008). Landslide-induced seeps are created by opening new structural and  
119 stratigraphical fluid pathways (Ranero et al. 2008; Mau et al. 2012) or by gas hydrate dissociation  
120 resulting from altered pressure and temperature conditions.

121 Fluids and related methane fluxes can vary both spatially and temporally as well as in origin,  
122 composition, and flow velocity. Temporal variations can be caused by gas hydrate formation and  
123 dissociation (Hesse et al. 2000; Tryon et al. 2002; Hensen et al. 2004; Minami et al. 2012) or triggered  
124 by earthquakes, which are frequent in this active subduction zone (Tryon et al. 2002; Hensen et al.  
125 2004; Aiello 2005; Henrys et al. 2006; Mau et al. 2007; Fischer et al. 2013).  
126 Well-known examples exhibiting such dynamics are the twin mounds "Mound 11" and "Mound 12",  
127 located at 1000 m water depth, halfway between the Nicoya and Osa Peninsulas. Both mounds are

Tina Treude 11.8.2015 13:56

**Gelöscht:** Because methane is an important greenhouse gas, it is not only our interest to quantify the efficiency of the benthic methane filter at steady state, but also the response of the filter to variable fluid flow conditions. To investigate the development of the geochemical gradients and dynamics under such conditions, as well the efficiency of the benthic microbial methane filter, we performed laboratory experiments with undisturbed seep sediments from Quepos Slide and exposed them to different flow conditions.

Tina Treude 12.8.2015 13:48

**Gelöscht:** huge

146 located at the same fault zone, although they differ in fluid flow advection intensity (Hensen et al.  
147 2004; Linke et al. 2005; Karaca et al. 2010; Krause et al. 2014), fluid origin (Hensen et al. 2004; Han et  
148 al. 2004; Schmidt et al. 2005), and microbial activity (Krause et al. 2014). In the last 50 kyr both  
149 mounds have displayed individual active phases interrupted by phases of inactivity (Kutterolf et al.  
150 2008). In contrast to this long term variability, Furi et al. (2010) observed a two month seepage event  
151 at Mound 11 with flow rates that varied four-fold (from 5 cm yr<sup>-1</sup> to 20 cm yr<sup>-1</sup>). Events like this affect  
152 the efficiency of the benthic microbial methane filter and result in increased methane concentrations  
153 in the water column. Slow adaptation to increased methane supply may explain elevated methane  
154 concentrations in the water column offshore Costa Rica found by Mau et al. (2007) in 2003,  
155 presumably caused by an earthquake earlier that year.

156 The research area of the present study, the Quepos Slide, is located south of the twin Mounds 11 and  
157 12. This landslide is approximately 9.5 km wide and 8 km long (Harders 2011). The translational slide  
158 has a headwall 160 m in height and the slide head is located at ~400 m water depth in the Eastern  
159 Pacific oxygen minimum zone (OMZ; between 250 -550 m water depth; Bohrmann et al. 2002). Four  
160 tongues of the landslide can be identified, reaching down to ~800 water depth, indicating three  
161 subsequent events following the initial slide (Bohrmann et al. 2002; Harders et al. 2011). The Quepos  
162 Slide was most likely caused by seamount subduction (Harders et al. 2011). Along the toe, fluids and  
163 gas can migrate from hydrates inside the GHSZ. Chemosynthetic organisms are abundant, with  
164 bacterial mats present throughout, while authigenic carbonates and clams can be found at deeper  
165 areas and at the toe of the slide (Bohrmann et al. 2002). Directly below the headwall, the sediments  
166 are covered by sulfur bacteria mats (Bohrmann et al. 2002; Sahling et al. 2008; Karaca et al. 2012).  
167 Empirical models show that vertical fluid flow at Quepos Slide varies between 1 and 40 cm yr<sup>-1</sup> and  
168 AOM rates vary between 1.5 and 42.1 mmol m<sup>-2</sup> d<sup>-1</sup> (Karaca et al. 2012). According to that model,  
169 53% (~316 x 10<sup>3</sup> mol yr<sup>-1</sup>) of the methane is oxidized by the highly active benthic microbial methane  
170 filter, while 47% (280 x 10<sup>3</sup> mol yr<sup>-1</sup>) is released into the water column. Elevated methane

Tina Treude 13.8.2015 16:04

**Gelöscht:** made

<sup>172</sup> concentrations of 72 nmol l<sup>-1</sup> was observed in the seawater directly above the slide head (Bohrmann  
<sup>173</sup> et al. 2002).

174 **2. Methods:**

175 Surface sediments from Quepos Slide were obtained by a video-guided multi-corer (TV-MUC) during  
176 the GEOMAR research cruise SO206 [in June 2010](#) on the German research vessel "SONNE". Two sites  
177 (SO206-29 MUC, SO206-31 MUC) from the headwall of Quepos Slide, both covered by sulfur bacteria  
178 mats, were sampled (Table 1). All subsampling procedures were performed on board at 4°C  
179 immediately after obtaining the sediments. Three replicate cores ([inner diameter 10 cm](#)) of each TV-  
180 MUC were used for (1) porewater analyses, (2) ex situ AOM and sulfate reduction rate assays, and (3)  
181 methane concentration determination. Additionally, two replicate cores of SO206-31 (MUC) were  
182 sub-sampled for laboratory experiments (SLOT-system, see below).

183 **2.1 Porewater measurement (ex situ):** Porewater of the ex situ samples was extracted by a pressure-  
184 filtration system and filtered (argon 3–4 bar, 0.2 µm regenerated cellulose filters, Krause et al. 2014).  
185 Total alkalinity (TA) was analyzed onboard via titration (Ivanenkov and Lyakhin 1978). Sulfide was  
186 determined photometrically [using the methylene blue method \(Cline 1969\)](#). Sub-samples for the  
187 determination of sulfate, chloride, and bromide were frozen and analyzed onshore by ion  
188 chromatography (Compact IC 761). Further porewater sampling and analytical procedures are  
189 described in detail by Krause et al. (2013).

190 **2.2 Methane (ex situ):** For methane determination, 10 cm<sup>3</sup> of sediment was transferred to [30 mL](#)  
191 glass vials filled with 10 ml 10% KCl for poisoning and headspace equilibration. [The methane](#)  
192 [concentration was determined on board by gas chromatography coupled to a flame ionization](#)  
193 [detector \(GC-FID\) using a Shimadzu GC14A instrument fitted with a Restek Rt®Alumina Bond/KCl](#)  
194 [capillary column \(50 m, 0.53 mm ID\) operated at 60 C. N2 was used as a carrier gas.](#)

195 **2.3 Microbial rate measurement (ex situ):** Ex situ turnover rates of sulfate reduction and AOM were  
196 determined with radiotracer techniques. For both sulfate reduction and AOM, three replicate  
197 polycarbonate tubes (26 mm inner diameter, 250 mm length) were sub-sampled from one TV-MUC  
198 core and incubated by whole core incubation (Jørgensen 1978). Additional bulk sediment was  
199 sampled to produce controls. Fifteen µl <sup>14</sup>CH<sub>4</sub> (1–2 kBq dissolved in anoxic, sterile water; specific

Tina Treude 11.8.2015 16:53

**Gelöscht:** by

Tina Treude 12.8.2015 14:08

**Gelöscht:** Methane concentrations were measured onboard using a Shimadzu GC14A gas chromatograph fitted with a Restek® Alumina Bond capillary column and operated with nitrogen as carrier gas.

208 activity 22.28 GBq mmol<sup>-1</sup>), and 6 μl <sup>35</sup>SO<sub>4</sub><sup>2-</sup> (200 kBq dissolved in water; specific activity 37 TBq mmol<sup>-1</sup>), was injected into the AOM and sulfate reduction cores, respectively, at a vertical resolution of 1  
209 cm; the cores were then incubated for 24 h in the dark at in situ temperature (8°C). After incubation,  
210 the sediment cores were sliced in 1 cm intervals and transferred to 20 ml NaOH (2.5% w/v, 40 ml glass  
211 vials with rubber stopper) for AOM, and 20 ml zinc acetate (20% w/v, 50 ml plastic vials) for sulfate  
212 reduction determinations. Control samples (five each), were first transferred to the respective  
213 chemicals before tracer was added (see above). AOM was determined according to Treude et al.  
214 (2005)(GC and Combustion) and Joye et al. (2004) (<sup>14</sup>CO<sub>2</sub> trapping). Sulfate reduction was determined  
215 using the cold chromium distillation method after Kallmeyer et al. (2004).  
216

217 **2.4 Numerical model:** Porewater profiles were simulated using a one-dimensional transport reaction  
218 model, previously used and described by Krause et al. (2013), to determine the flow velocity of the  
219 fluid and the rate of AOM. Carbonate precipitation was implemented in the model (Krause et al.,  
220 2013) but was not used in the present study for simplicity, since carbonate precipitation does not  
221 affect the efficiency of the microbial benthic methane filter within the studied time scales (several  
222 months to years). Because the sampling sites were located above the GHSZ (Wallmann et al. 2012),  
223 dissolved methane concentrations at the lower boundary were calculated from the equilibrium  
224 concentration with free gas (Tishchenko et al. 2005). Table 2 provides an overview of other boundary  
225 conditions as well as fitted, measured, and calculated parameters of the model.

226 **2.5 Sediment-Flow-Through System:** The response of the sediment to changes in fluid and methane  
227 fluxes was studied using a newly-developed Sediment-Flow-Through (SLOT)-system (Steeb et al.  
228 2014), which mimics natural flow conditions with diffusive supply of sulfate at the sediment surface  
229 and advective methane supply at the bottom of the core. The system enables continuous monitoring  
230 of geochemical gradients inside the sediment as well as in the in- and outflow and allows the  
231 development of the geochemical gradients and SMTZ to be observed. The efficiency of the benthic  
232 microbial methane filter during the transient periods can be calculated from the measured input and  
233 output fluxes (see below). For the present study we focused only on AOM, i.e., all incubations were

Tina Treude 12.8.2015 13:50

Gelöscht: s

Tina Treude 11.8.2015 18:59

Gelöscht: 4

236 kept strictly anoxic, as AOM is the most important process for methane removal in the sediment. The  
237 system has limitations, as it is not pressurized and therefore does not generate methane  
238 concentrations found in situ. The mere interest for using it was to study the response of AOM and  
239 the SMTZ to different fluid flow rates, which should always be kept in mind when interpreting the  
240 results. Please refer to Steeb et al. 2014 for more details on the method's advantages and  
241 disadvantages.

242 For SLOT experiments, two replicate multicorer cores from station SO206-31 (MUC) were sub-  
243 sampled with specific SLOT liners (inner diameter 6 cm) (Steeb et al. 2014). Liners were closed with  
244 rubber stoppers, sealed with electrical tape, transported (4°C) to the home laboratory and stored at  
245 0°C in the dark until the experiment started (ca. 170 days after the MUC sampling). At GEOMAR,  
246 filters (glass fiber, Whatman GF/F) were applied at the bottom of the sediment core and at the lower  
247 and upper cap, as previously described (Steeb et al. 2014).

248 The following experimentations were conducted at 10°C (the in situ temperature was 8°C). Two  
249 different seawater media were applied: one medium, resembling seawater, was amended to natural  
250 sulfate concentrations (28 mmol l<sup>-1</sup>). The added sulfate penetrated the sediment by diffusion, except  
251 for when porewater subsamples were taken with rhizons (see below), which temporarily facilitated a  
252 faster intrusion of sulfate-rich water from the supernatant and probably caused a smoothing of  
253 porewater profiles (Steeb et al. 2014). The other medium, resembling sulfate-free seepage fluid,  
254 carried dissolved methane (965 ± 180 μmol l<sup>-1</sup>) upwards into the bottom of the core by advection.  
255 Both media were based on the sulfate reducer medium developed by Widdel and Bak (2006). In the  
256 "seepage" medium, MgSO<sub>4</sub> was replaced by MgCl. Both media were kept anoxic, and contained  
257 resazurin as oxygen indicator (Visser et al. 1990), with a pH adjusted to 7.5 and a salinity of 35 PSU.  
258 Bromide served as an inert tracer for the upward migration and was present only in the methane-  
259 enriched seepage medium (800 μmol l<sup>-1</sup>). Hence, the depth where bromide and sulfate  
260 concentrations overlapped was interpreted as the SMTZ. We therefore used the sulfate-bromide  
261 transition zone (SBTZ) as a proxy for the SMTZ and defined it as the zone with the steepest SO<sub>4</sub><sup>2-</sup> and

Tina Treude 11.8.2015 18:32

**Gelöscht:** and

Tina Treude 13.8.2015 13:20

**Gelöscht:** for transport.

264 Br<sup>-</sup> gradients. Medium composition and the gas headspace composition of the reservoirs are  
265 summarized in [Table 3](#),  
266 SLOT experiments were performed with two sediment cores under different flow regimes ([Table 4](#)).  
267 One core was exposed to a relatively moderate advective fluid flow velocity (10.6 cm yr<sup>-1</sup>), here  
268 further referred as the low flow core (LFC), whereas the other core was exposed to a 10-fold higher  
269 advective fluid flow velocity (106.3 cm yr<sup>-1</sup>), further referred as the high flow core (HFC). The  
270 moderate fluid flow velocities were on the same order as those determined by the numerical model  
271 (see Results). The high flow velocities were more than twice of those previously reported for Quepos  
272 Slide (40 cm yr<sup>-1</sup>; Karaca et al. 2012) and were employed to observe the sediment response under  
273 extreme fluid flow. Similar or even higher (up to 200 cm yr<sup>-1</sup>) advective flow velocities have been  
274 reported for seeps within the same region (Hensen et al. 2004; Linke et al. 2005; Karaca et al. 2010;  
275 Krause et al. 2014). The applied fluid flow velocities were strong enough to observe considerable  
276 changes within the time frame of one year yet weak enough to avoid sulfate penetration to less than  
277 one cm.  
278 In the initial preparation phase of the experiment (40 days), the outflow of the system was located at  
279 the bottom of the core and only methane-free seawater medium was pumped from top to bottom [at](#)  
280 [a pump rate of 20 µl min<sup>-1</sup>](#). This procedure was applied to establish a homogeneous sulfate  
281 distribution and anoxic conditions throughout the entire sediment column without disturbing the  
282 sediment fabric, [although some sediment compaction might occur](#). In the subsequent first  
283 experimental phase, the outflow was mounted at the top of the core and seawater medium was  
284 delivered to the overlying seawater at a pump rate of 20 µl min<sup>-1</sup>. From this point, sulfate was  
285 transported into the sediment core solely via diffusion, [except for rhizon sampling \(see above\)](#). From  
286 the bottom, the seepage medium was supplied at 0.5 µl min<sup>-1</sup> (LFC) and 5 µl min<sup>-1</sup> (HFC) with an  
287 average inflow methane concentration of 965 ± 180 µmol l<sup>-1</sup>. Based on the pump rate, methane  
288 concentration, and surface area of the sediment, a methane flux of 0.28 and 2.81 mmol m<sup>-2</sup> d<sup>-1</sup> was  
289 calculated for the LFC and HFC core, respectively. These methane concentrations were lower than

Tina Treude 11.8.2015 18:58

Gelöscht: t

Tina Treude 11.8.2015 19:00

Gelöscht: 2

Tina Treude 12.8.2015 17:17

Gelöscht: .

293 those potentially encountered under in situ conditions because the cores were not pressurized,  
 294 resulting in lower methane fluxes (after Tishchenko et al. 2005; Karaca et al. 2012). After 260 d the  
 295 first experimental phase ended and the pump rates were increased from low to high flow velocities  
 296 for the LFC, and vice versa for the HFC. This switch marked the beginning of the second and final  
 297 experimental phase to study the response of AOM to rapid changes in the flow regime. After 316 d,  
 298 the experiment was terminated and the cores were sliced and sub-sampled for further analyses (see  
 299 below).

300 Methane emission from the sediment was calculated by multiplying the out-flow methane  
 301 concentrations ( $CH_{4out}$ ) with the dilution factor (DF; 41 and 5 for LFC and HFC, respectively) and the  
 302 fluid flow ( $v$ ; 10.6 and 106.3  $cm\ yr^{-1}$  for LFC and HFC, respectively) according to equation (1).

$$303 \quad CH_{4_{efflux}} [mmol\ m^{-2}\ d^{-1}] = v [cm\ yr^{-1}] \cdot CH_{4_{out}} [mmol\ cm^{-3}] \cdot DF \cdot \frac{10\ 000}{365.25} \quad (1)$$

304 Areal AOM rates ( $AOM_{areal}$ ) were calculated from the difference between in- ( $CH_{4in}$ ) and outflow  
 305 ( $CH_{4out}$ ) methane concentrations before (258 d) and after (316 d) fluid flow velocity change according  
 306 to equation (2),

$$307 \quad AOM_{areal} [mmol\ m^{-2}\ d^{-1}] = \left( \frac{CH_{4in} [mmol\ cm^{-3}] - CH_{4out} [mmol\ cm^{-3}] \cdot DF}{HRT [d]} \right) \cdot \frac{10\ 000}{SLOT_{base} [cm^2]} \quad (2)$$

308 with  $SLOT_{base}$  for the base area of the SLOT-cores and DF for the dilution factor in the overlying water,  
 309 resulting from the different pump rates for the “seepage” and “seawater” media and their mixing in  
 310 the overlying water. HRT stands for the hydrological residence time, the average time of the seepage  
 311 medium to flow from the core inflow, through the sediment column, to the core outflow, and was  
 312 calculated by dividing the water volume above and below the sediment core plus the sediment  
 313 porewater volume by the flow rate.

Tina Treude 13.8.2015 14:50  
**Gelöscht:** through the  
 Tina Treude 13.8.2015 14:50  
**Gelöscht:**

316 **2.6 Geochemical parameters during SLOT experimentation:** During the SLOT experiments,  
317 geochemical parameters were measured in 1 cm depth intervals throughout the sediment core. In  
318 addition, concentrations in the in- and out-flowing fluids were monitored. Sulfide concentrations, pH,  
319 and redox potential were measured with microsensors (sulfide needle sensor, H<sub>2</sub>S-N, tip diameter 0.8  
320 mm, Unisense; pH, MI 411 B, Gauge 20, Microelectrodes Inc.; redox potential needle sensors, MI-  
321 800, Gauge 25, Microelectrodes Inc.). Porewater samples (1.5 – 2 ml) for the determination of  
322 sulfate, bromide, and total alkalinity were obtained from each depth in the sediment using pre-  
323 installed rhizones (CSS-F, length 5 cm, diameter 2.5 mm, pore size 0.2 µm, Rhizosphere®). The in- and  
324 outflow of both cores were sampled with glass syringes for the determination of sulfate, bromide,  
325 total alkalinity and methane concentration. All sampling and measurement proceedings for the  
326 experiment are described in detail by Steeb et al. (2014). Given a removal of 8.1% porewater during  
327 each rhizon sampling, which causes mixing with adjacent layers, and an analytical precision of <1%  
328 (ion chromatography) and 0.1% (total alkalinity titration), we estimated a total analytical error of ca.  
329 9% for sulfate and bromide, and 8.2% for total alkalinity, respectively.

### 330 **2.7 Experiment termination and final sampling:**

331 At the end of the experiment, 1.5 ml porewater from each depth was sampled for determinations of  
332 sulfide (0.5 ml), sulfate and bromide (0.5 ml) as well as total alkalinity (0.5 ml), and analyzed after the  
333 same methods as the ex situ porewater (see section 2.1).

334 After the final porewater sampling, sediment sub-samples were taken from each SLOT core. Two sub-  
335 cores (polycarbonate, length 260 mm, inner diameter 26 mm) were collected from each SLOT core  
336 for radiotracer determinations of AOM and sulfate reduction, and treated according to the protocols  
337 mentioned above. For the determination of methane concentrations, each SLOT core was sampled in  
338 1 cm intervals (2 cm<sup>3</sup> volume sub-samples) using cut-off syringes (3 ml, PE). The sediment samples  
339 were transferred into glass vials (13 ml) with 5 ml 2.5% w/v NaOH. Vials were closed with butyl  
340 rubber stoppers and shaken directly after sampling. Methane was analyzed by gas chromatography  
341 (Hewlett Packard Series II) with a packed column (Haye SepT, 6 ft, 3.1 mm inner diameter, 100/120

Tina Treude 13.8.2015 13:27

Gelöscht: 1.0

343 mesh, Resteck, carrier gas: He 20 ml min<sup>-1</sup>, combustion gas: synthetic air 240 ml min<sup>-1</sup>, H<sub>2</sub> 20 ml min<sup>-1</sup>).

344 1).

345 The remaining sediment of each SLOT core was sampled in 2 cm depth intervals. For porosity

346 measurements, approximately 2 cm<sup>3</sup> samples were obtained using cut-off syringes (3 ml, PE),

347 transferred to pre-weighed vials, and weighed, before and after the sample was freeze-dried.

348 Porosity was then calculated by the difference in weight (Dalsgaard et al. 2000). Sub-samples of the

349 dried sediment were used to determine total carbon (TC), total nitrogen (TN), total sulfur (TS) and

350 total organic carbon (TOC) of the solid phase. TC, TN, TS, and TOC were analyzed using a CARLO ERBA

351 Elemental Analyzer NA 1500. For TOC determination, inorganic carbon was removed by adding

352 hydrochloric acid. Total inorganic carbon (TIC) was calculated from the difference between TC and

353 TOC. All solid phase analyses were carried out in duplicates.

354 Further details on the SLOT sampling procedure and analytical procedures are described in Steeb et

355 al. (2014).

356

### 3. Results:

#### 3.1 Ex situ profiles and numerical models

Both MUC cores (SO206-29 MUC and SO206-31 MUC) were sampled at ~ 400 m water depth from sediments covered with sulfur bacteria mats, which are indicative for high methane fluxes (Torres et al. 2002; Treude et al. 2003).

At station SO-206-29 (MUC), sulfate decreased from 28 mmol l<sup>-1</sup> at the sediment surface to zero at the bottom of the core (26 cm below sea floor (cmbsf)) (Fig. 1, A). Conversely, methane concentrations were low (0.0 – 0.1 mmol l<sup>-1</sup>) in the upper 15 cmbsf and increased below this zone to a maximum of 2.4 mmol l<sup>-1</sup> at the bottom (Fig. 1, A). Accordingly, the SMTZ was located at approximately 17.5 cmbsf. Two maxima in sulfate reduction rates were identified in one of the replicate cores at the top (up to 1821 nmol cm<sup>-3</sup> d<sup>-1</sup>) and between 12.5 and 22.5 cmbsf (up to 879 nmol cm<sup>-3</sup> d<sup>-1</sup>) (Fig. 1, B). AOM coincided with the second sulfate reduction maximum and reached rates up to 569 nmol cm<sup>-3</sup> d<sup>-1</sup> (Fig. 1, C). Sulfide and total alkalinity (TA) increased from the top (0.0 mmol l<sup>-1</sup> and 2.5 meq l<sup>-1</sup>, respectively) to a maximum within the SMTZ (7.9 mmol l<sup>-1</sup> and 23.4 meq l<sup>-1</sup>, respectively, at 17.5 cm sediment depth), (Fig. 1, D). Areal turnover rates of methane and sulfate integrated over the entire sediment depth of 26 cm were similar for AOM (on average 12.87 ± 5.98 mmol m<sup>-2</sup> d<sup>-1</sup>) and sulfate reduction (on average 13.38 ± SD 13.61 mmol m<sup>-2</sup> d<sup>-1</sup>) with a ratio of 0.96 (AOM : sulfate reduction), respectively.

The steady state model resulted in a fluid flow of 7 cm yr<sup>-1</sup> and an areal AOM rate of 11.35 mmol m<sup>-2</sup> d<sup>-1</sup> (Table 2). In total, around 92% of the delivered methane was oxidized by AOM and ~8% was released to the seawater. Fitted porewater profiles and AOM rates are shown in Fig. 1.

In the second core, SO206-31 (MUC), sulfate decreased to 0 mmol l<sup>-1</sup> within the first 15 cm sediment depth and considerable methane concentrations (> 3.4 mmol l<sup>-1</sup>) were observed at 5 cmbsf (Fig. 2, A).

The observed maximum methane concentration was 10.2 mmol l<sup>-1</sup> (20.5 cmbsf). Accordingly, the SMTZ was located at approximately 5 - 15 cmbsf. Sulfate reduction and AOM occurred between 0 and 12.5 cmbsf with a sulfate reduction maximum (12052 nmol cm<sup>-3</sup> d<sup>-1</sup>) at the top of the SMTZ (~2.5

Tina Treude 10.8.2015 17:02

Gelöscht: 4

Tina Treude 10.8.2015 17:02

Gelöscht: yr

Tina Treude 11.8.2015 19:00

Gelöscht: 4

386 cmbsf) and an AOM maximum ( $1400 \text{ nmol cm}^{-3} \text{ d}^{-1}$ ) in the upper part of the SMTZ (5.5 cm cmbsf)  
387 (Fig. 2, B, C). Highest sulfide and TA concentrations were measured within the SMTZ between 10 and  
388 15 cmbsf ( $8.6 \text{ mmol l}^{-1}$  and  $24.1 \text{ meq l}^{-1}$ , respectively) (Fig. 2, D). Areal sulfate reduction rates  
389 integrated over the entire sediment depth of 25 cm ( $218.90 \pm 159.80 \text{ mmol m}^{-2} \text{ d}^{-1}$ ) were around 5  
390 times (AOM : SR = 0.21) higher compared to the areal rates of AOM ( $45.15 \pm 11.48 \text{ mmol m}^{-2} \text{ d}^{-1}$ )  
391 integrated over of the same depth.

392 Replicate cores from SO206-31 taken for porewater and rate analyses showed a different depth of  
393 the SMTZ and the AOM peak, respectively. Based on this lateral heterogeneity, two different fits of  
394 AOM were applied in the numerical model, one for the porewater core (pw-fit) and one for the rate  
395 core (hf-fit), which required a higher fluid advection to align the modeled and measured AOM,  
396 (details see Table 2). The pw-fit with  $7 \text{ cm yr}^{-1}$  fluid flow showed an efficient benthic filter which  
397 oxidized all delivered methane ( $9.09 \text{ mmol m}^{-2} \text{ d}^{-1}$ ). The hf-fit ( $29 \text{ cm yr}^{-1}$ ) had an AOM rate of  $41.69$   
398  $\text{mmol m}^{-2} \text{ d}^{-1}$  and oxidized around 93% of the delivered methane ( $45.09 \text{ mmol m}^{-2} \text{ d}^{-1}$ ). Model results  
399 are shown in Fig. 2 and summarized in Table 2.

### 401 3.2 SLOT incubation experiments

402 For the SLOT-Incubations, two replicate cores from SO206-31 (MUC) were used.

#### 403 3.2.1 Evolution of biogeochemical parameters during the main phase of the experiment (0-260 404 days):

##### 405 *The low fluid flow regime core*

406 In the low flow regime core (LFC) incubations, **bromide** concentration, which was used as a tracer to  
407 track the seepage medium, was always very low and near detection limit ( $20 \mu\text{mol l}^{-1}$ ). Values  
408 increased only weakly in the lowest 5 cm of the core, reaching a maximum of  $45 \mu\text{mol l}^{-1}$  after 49 d  
409 (Fig. 3 D). After 105 d, a small concentration of bromide ( $< 3 \text{ mmol l}^{-1}$ ) appeared in the supernatant,  
410 which later (171 d) disappeared again. Sulfate, which was delivered from the top by diffusion,  
411

Tina Treude 13.8.2015 12:41

**Gelöscht:** from SO206-31

Tina Treude 12.8.2015 12:42

**Gelöscht:** ce in

Tina Treude 12.8.2015 12:38

**Gelöscht:** for

Tina Treude 12.8.2015 12:38

**Gelöscht:** ;

Tina Treude 12.8.2015 12:42

**Gelöscht:** another

Tina Treude 12.8.2015 12:42

**Gelöscht:** where the model simulated instead the rates

Tina Treude 13.8.2015 12:44

**Gelöscht:** (hf-fit)

Tina Treude 11.8.2015 19:01

**Gelöscht:** 4

Tina Treude 12.8.2015 17:52

**Formatiert:** Hochgestellt

421 decreased only slightly at the bottom of the core ( $27.2 \text{ mmol l}^{-1}$ ) due to a slow advection of methane-  
422 enriched seepage medium. This was in accordance with the small increase in bromide (up to  $\sim 45$   
423  $\mu\text{mol l}^{-1}$ ). After 105 d, sulfate levels stabilized around  $26 \text{ mmol l}^{-1}$  at the bottom of the core and did  
424 not further decrease during the low flow phase.

425 In the first 105 d, **sulfide** concentrations of the LFC core varied between  $23$  and  $300 \mu\text{mol l}^{-1}$  over  
426 depth with a maximum between  $9 - 11 \text{ cm}$  (Fig. 3 B, E, H). After 171 d, a sulfide peak ( $920 \mu\text{mol l}^{-1}$ ,  
427 Fig. 3 K) occurred at  $0.26 \text{ cm}$  sediment depth, while no sulfide was detected in the overlying water.  
428 Below the peak, sulfide varied between  $300$  and  $500 \mu\text{mol l}^{-1}$ . Thirty days later (201 d runtime),  
429 maximum sulfide concentrations of up to  $230 \mu\text{mol l}^{-1}$  were observed between  $1.5$  and  $10.7 \text{ cm}$   
430 sediment depth (Fig. 3 N). After 258 d, directly before changing from low to high fluid flow, maximum  
431 sulfide concentrations were  $115 \mu\text{mol l}^{-1}$  at  $4.5\text{-}5.5 \text{ cm}$  (Fig. 3, Q) and decreased to a minimum of  
432  $36 \mu\text{mol l}^{-1}$  near the sediment-water interface.

433 **Total Alkalinity (TA)** was predominantly lower inside the cores than in the media ( $30 \text{ meq l}^{-1}$ ). During  
434 the LFC incubation, TA continuously decreased over the time from  $\sim 30$  to  $\sim 24 \text{ meq l}^{-1}$  below  $\sim 9 \text{ cm}$   
435 (Fig. 3, B, E, H, K). After 171 d, TA varied between  $28.7$  and  $21.7 \text{ meq l}^{-1}$ . Directly before the change of  
436 fluid flow (258 d), TA increased from the top ( $23.3 \text{ meq l}^{-1}$ ) to the bottom ( $26.7 \text{ meq l}^{-1}$ ; Fig. 3, Q).

437 Initial **redox potential** of the LFC was  $-50 \text{ mV}$  at the top and around  $-150 \text{ mV}$  below  $2 \text{ cm}$  sediment  
438 depth (Fig. 3 C). After 49 d, the redox potential was more negative ( $-130 \text{ mV}$  at top and between  $-160$   
439 to  $-270 \text{ mV}$  below, Fig. 3, F); after 105 d, the redox potential increased to  $-80 \text{ mV}$  at the top (Fig. 3, I).

440 Between 171 and 202 d runtime, the overlying water of the core showed a pink color caused by the  
441 oxygen indicator resazurin. At the same time, the redox potential was positive (between  $150$  and  $100$   
442  $\text{mV}$ ) at the sediment water interface (Fig. 3 L, O), probably as a result of oxygen intrusion.

443 Nevertheless, free oxygen should result in a redox potential  $>350 \text{ mV}$  (Schulz 2000). We therefore  
444 assume that oxygen was only temporally available and rapidly consumed. Deeper inside the  
445 sediment, redox potential reached values between  $-200$  and  $-400 \text{ mV}$  (Fig. 3 L, O).

446 Directly before changing the fluid flow (258 d), the redox potential of the LFC was -100 mV in the  
447 overlying water and around -200 mV inside the sediment (Fig. 3 R).

448 After 171 d runtime, **pH** was highest at the sediment-water interface (8.2, Fig. 3 L) and around 7.6  
449 deeper in the sediment. Final pH before fluid flow swapping (258 d) decreased from 7.6 at the top to  
450 7.1 at the bottom of the core (Fig. 3 R).

451 **Methane** concentrations in the out-flow of the LFC started at  $1.5 \mu\text{mol l}^{-1}$  (29 d) and increased to  $2.5$   
452  $\mu\text{mol l}^{-1}$  after 105 d before decreasing again to  $0.9 \mu\text{mol l}^{-1}$  after 258 d (Fig. 5). Calculated methane  
453 efflux followed the methane concentration trend. The LFC methane efflux was between 0.011 and  
454  $0.030 \text{ mmol m}^{-2} \text{ d}^{-1}$ . AOM rates from the difference of in- and out-flow were  $0.304 \text{ mmol m}^{-2} \text{ d}^{-1}$ ,  
455 directly before changing the fluid flow regime. However, this rate must overestimate the actual AOM  
456 activity, because the core did not reach steady state before the fluid flow change, as the bromide  
457 front did not reach the sediment-water interface (see discussion).

458

459 *The high fluid flow regime core:*

460 In the high flow regime core (HFC), **bromide** quickly appeared after 21 d ( $400 \mu\text{mol l}^{-1}$ ) at the bottom  
461 of the core (Fig. 4, A). Bromide concentration continuously increased from the bottom towards the  
462 top of the core until a chemocline developed between 4 and 10 cm sediment depth after 105 d (Fig.  
463 4, G). This chemocline persisted during the remaining experiment and moved slowly upwards  
464 reaching a zone between 1 and 6 cm depth after 258 d (Fig. 4, A, D). **Sulfate** concentrations during  
465 the HFC period were opposite to the bromide distribution and coincided with the chemocline. Sulfate  
466 continuously decreased towards the bottom of the core reaching the minimum concentration  
467 ( $0.2 \text{ mmol l}^{-1}$ ) after 201 d (Fig. 4, M). Simultaneously, sulfate was more and more displaced from the  
468 bottom to the top of the core, decreasing from  $28.5 \text{ mmol l}^{-1}$  to  $12 \text{ mmol l}^{-1}$  at the sediment-water  
469 interface.

470 **Sulfide** concentrations were considerably lower compared to the LFC. At the beginning (21 d), sulfide  
471 increased from the top ( $27 \mu\text{mol l}^{-1}$ ) to 6 cm sediment depth ( $70 \mu\text{mol l}^{-1}$ ) within the developing SBTZ

472 (Fig. 4, B), which was used as proxy for the SMTZ, and was constant at this level below 6 cm sediment  
473 depth. In the following months, sulfide decreased below  $20 \mu\text{mol l}^{-1}$  (105 d) and increased rapidly  
474 after 171 d runtime at the top of the core to more than  $500 \mu\text{mol l}^{-1}$  (Fig. 4, K). In the following  
475 months, sulfide concentrations decreased again at first to maximum values of  $300 \mu\text{mol l}^{-1}$  (4 cm  
476 sediment depth, 202 d runtime) and to less than  $60 \mu\text{mol l}^{-1}$  after 258 d (Fig. 4, Q).

477 **TA** in the HFC core showed similar trends as the LFC core. Near the start (21 d), TA decreased from 29  
478 to  $30 \text{ meq l}^{-1}$  at the top of the core to  $26 - 27 \text{ meq l}^{-1}$  at the bottom (Fig. 4, B, E, H). After 171 d, this  
479 distribution reversed with TA increasing from the top of the core to the bottom, from  $21 - 26 \text{ meq l}^{-1}$   
480 to  $24 - 27 \text{ meq l}^{-1}$  (Fig. 4, K).

481 The **redox potential** of the HFC core was, similar to the LFC core, highest at the sediment-water  
482 interface and in the overlying water and lowest at larger depths of the core. Initially (21 d), redox  
483 potential was  $-85 \text{ mV}$  at the sediment water interface and between  $-100$  and  $-150 \text{ mV}$  in the  
484 sediment (Fig. 4, C). Over time, the redox potential in the sediment became more negative, reaching  
485 a value down to  $-385 \text{ mV}$  after 105 d (Fig. 4 I, L). Between 105 to 202 d runtime, the overlying water  
486 turned pink and showed a redox potential ranging from  $100$  to  $200 \text{ mV}$  (Fig. 4, Q), indicating oxygen  
487 contamination in the core. Directly before the change in fluid flow, the redox potential returned to  
488 negative values with  $-120 \text{ mV}$  in the overlying water and around  $-200 \text{ mV}$  in remaining core (Fig. 4, R).

489 Similar to the LFC core, the **pH** was highest at the sediment-water interface and lower inside the  
490 sediment ( $8.1 - 7.8$  after 171 d and  $8.0 - 7.4$  after 202 d; Fig. 4, L and O). Directly before the fluid  
491 flow change (258 d), pH decreased to  $7.6$  at the sediment water interface and to  $7.1-7.3$  inside the  
492 sediment (Fig. 4, R).

493 **Methane** concentration in the HFC outflow was initially (21 d)  $7.5 \mu\text{mol l}^{-1}$  and then decreased to  
494  $1.7 \mu\text{mol l}^{-1}$  during the following 200 d. After 258 d runtime, methane concentration in the outflow  
495 increased again to  $2.8 \mu\text{mol l}^{-1}$ . Efflux of the HFC ranged from  $0.025$  up to  $0.109 \text{ mmol m}^{-2} \text{ d}^{-1}$ .

496 Corresponding calculated AOM rates were  $3.114 \text{ mmol m}^{-2} \text{ d}^{-1}$  directly before changing the flow rate  
497 (258 d).

498 **3.2.2 Biogeochemical responses after changing the fluid flow regime (260-350 d runtime):**

499 After 260 d, the fluid flow in the cores was swapped from low to high and vice versa.

500 *New high flow regime core*

501 In the new high flow regime core (NHFC, *former LFC*) sulfate and bromide concentrations did not  
502 change considerably over the entire runtime (350 d). TA remained constant at 25 meq l<sup>-1</sup> (Fig. 3 T).

503 Sulfide concentrations were highest at 0.3 cm sediment depth (1230 μmol l<sup>-1</sup>) and first decreased  
504 steeply followed by a more steady increase (below 3 cm) with the exception of a second maximum  
505 (625 μmol l<sup>-1</sup>) at 5 cm. At the bottom of the core, a sulfide concentration of max 75 μmol l<sup>-1</sup> was  
506 reached. Redox potential was positive (31 mV) in the overlying water and between -280 and -330 mV  
507 within the sediment (Fig. 3 U). The pH decreased from 8.5 to 7.5 between the sediment-water  
508 interface and the bottom of the core.

509 Methane concentration of the outflow increased considerably from 0.9 to 11.6 μmol l<sup>-1</sup> after 316 d  
510 run time (Fig. 5). Calculated methane effluxes were 0.165 mmol m<sup>-2</sup> d<sup>-1</sup> and corresponding AOM rates  
511 were 2.970 mmol m<sup>-2</sup> d<sup>-1</sup>. Similar to the LFC, the AOM rate is most likely overestimated, as the core  
512 did not reach steady state (see discussion).

513 *New low flow regime core*

514 In the new low flow regime core (NLFC; *former HFC*), sulfate penetrated deeper and bromide  
515 ascended less into the sediment, as compared to the profile prior to fluid flow change (Fig. 4, S).

516 Sulfide concentrations remained low, between 50 and 80 μmol l<sup>-1</sup>, and TA varied between 23 and 25  
517 meq l<sup>-1</sup> (Fig. 4, T). Redox potential was positive (150 mV) at the sediment water interface and the  
518 upper sediment (Fig. 4, U). Below 2 cm sediment depth, redox decreased to values between -200 and  
519 -400 mV. The pH profile decreased from 8.05 in the overlying water and at the sediment-water  
520 interface down to 7.55 below 6 cm sediment depth.

521 Methane concentrations in the outflow declined from 2.8 to 0.7 μmol l<sup>-1</sup> (Fig. 5). Calculated methane  
522 effluxes were 0.009 mmol m<sup>-2</sup> d<sup>-1</sup> with a corresponding AOM rate of 0.306 mmol m<sup>-2</sup> d<sup>-1</sup>.

523

### 524 3.2.3 Biogeochemical parameters after experiment termination:

525 After 350 d runtime, the experiment was terminated, porewater was sampled, and the sediment sub-  
526 sampled for further analyses. In both cores, methane concentrations determined after experiment  
527 termination (around  $2.5 \mu\text{mol l}^{-1}$ ) were only a minor fraction of the original inflow concentration ( $965$   
528  $\mu\text{mol l}^{-1}$ ), which was probably mostly attributed to methane losses during porewater extraction using  
529 rhizones directly before sediment sampling (Steeb et al. 2014). In the NHFC (= former LFC) methane  
530 concentrations varied between 2 and  $4 \mu\text{mol l}^{-1}$  with a slight increase towards the bottom of the core  
531 (Fig. 6, A). Sulfate concentrations decreased slightly from  $29.5 \text{ mmol l}^{-1}$  at the top to  $26.2 \text{ mmol l}^{-1}$  at  
532 the bottom of the core (Fig. 6, B). Sulfide increased from  $50 \text{ mmol l}^{-1}$  at the sediment surface (0.3 cm)  
533 to a maximum of  $125 \mu\text{mol l}^{-1}$  at 6 cm and decreased to  $80 \mu\text{mol l}^{-1}$  at the bottom of the core (Fig. 6,  
534 C). AOM rates of the NHFC determined by radiotracer techniques showed highest values between 4  
535 to 10 cm sediment depth ( $0.50 - 0.91 \text{ nmol cm}^{-3} \text{ d}^{-1}$ ) and, in addition, increased from top ( $0.10 \text{ nmol}$   
536  $\text{cm}^{-3} \text{ d}^{-1}$ ) to bottom ( $0.33 \text{ nmol cm}^{-3} \text{ d}^{-1}$ ). Areal turnover rates of methane and sulfate integrated over  
537 the entire sediment core (0-15 cm) were  $0.043$  and  $2.31 \text{ mmol m}^{-2} \text{ d}^{-1}$  for AOM and sulfate reduction,  
538 respectively.

539 In the NLFC (= former HFC), methane concentrations remained consistently low at around  $2-4 \mu\text{mol l}^{-1}$   
540 (Fig. 7, A). Sulfate was between 27 and  $28.5 \text{ mmol l}^{-1}$  within the upper first 6 cm and then decreased  
541 to  $10 \text{ mmol l}^{-1}$  below this depth (Fig. 7, B). Consistent with the steepest decrease in sulfate, sulfide  
542 increased to a maximum of  $42 \mu\text{mol l}^{-1}$ . Highest AOM rates determined with radiotracer techniques  
543 were detected between 5 and 11 cm ( $0.4 - 1 \text{ nmol cm}^{-3} \text{ d}^{-1}$ , Fig. 7, A). Sulfate reduction rates ranged  
544 from  $16.95$  to  $27.71 \text{ nmol cm}^{-3} \text{ d}^{-1}$  in the upper sediment (0 - 6 cm depth) and decreased to  
545  $7.96 \text{ nmol cm}^{-3} \text{ d}^{-1}$  at the bottom, which corresponded to a simultaneous decrease in sulfate at the  
546 bottom of the core (Fig. 6, A). Areal rates integrated over the entire sediment depth (14 cm) were  
547  $0.042$  and  $2.494 \text{ mmol m}^{-2} \text{ d}^{-1}$  for AOM and sulfate reduction, respectively.

548 The TC contents were similar in both, the NHFC and NLFC core, and varied between 4.97 and 6.05 dry  
549 wt.% (Fig. 8, A, Fig. 9 A). A carbon peak (6.05 dry wt.%, 7 cm sediment depth) resulted from higher

550 TIC (3.09 -3.16 dry wt.%) in both cores. TOC (2.90 – 3.62 dry wt.%) of the NHFC and NLFC did not  
551 differ considerable from ex situ data (2.91–3.40 dry wt.%). Atomic C/N ratios were higher in both  
552 flow-through cores (8.67 – 9.43) compared to ex situ values (7.61 – 8.88), while TS was slightly lower  
553 (0.82 – 1.18 compared to 0.94 - 1.27 dry wt.%), especially in the upper region (0 - 2 cm) of the NHFC  
554 (0.84 compared to 1.11 dry wt.%) and showed, in contrast to the ex-situ cores, no minimum at 4.5  
555 cm sediment depth (Fig. 8, C; Fig. 9, C).

## 4. Discussion:

### 4.1 The impact of fluid seepage and related processes on porewater gradients:

Quepos Slide sediment cores that were studied ex situ showed a SMTZ and AOM peaks within the upper 20 cm of the sediment (Fig. 2). We are therefore confident that the SLOT experiments (core length 14-16 cm) contained the most active zone of the benthic methane filter. During the experiments, the depth of the SBTZ, as proxy for the SMTZ, was controlled by fluid flow and migrated over time. Fluid flow velocity in the low flow regime core (LFC,  $10.6 \text{ cm yr}^{-1}$ ) was in the same range of fluid flow modeled from the ex situ data ( $5\text{-}29 \text{ cm yr}^{-1}$ ). In the high flow regime core (HFC,  $106 \text{ cm yr}^{-1}$ ), the fluid flow was two to ten times higher compared to our modeled data and also higher than other values published for Quepos Slide ( $1\text{-}40 \text{ cm yr}^{-1}$ , Karaca et al. 2012, Table 5); however, the flow was still in the range of neighboring seeps ( $0.1\text{--}200 \text{ cm yr}^{-1}$ , Hensen et al. 2004; Linke et al. 2005; Karaca et al. 2010; Krause et al. 2013). During the entire LFC/NHFC experiment, no SBTZ developed, and consequently no steady state was reached. The missing evolution of a SBTZ was probably the result of a high hydrological residence time of the seepage medium (696 d for the LFC and 69 d for the NHFC), which in this case means the average time for the fluid to pass the water volume below the core and the entire sediment core. Nevertheless, small amounts of the seepage fluid obviously passed through the entire sediment, probably facilitated through channeling (Torres et al. 2002; Wankel et al. 2012), as demonstrated by the presence of methane in the outflow (Fig. 5) and bromide in the supernatant (Fig. 3G). The fraction of seepage medium (calculated from  $\text{Br}^-$  concentration) emitted, relative to the total inflow seepage volume of the LFC, increased from 0% to 2.5% in the last phase (260 d) and further increased to 4% after the system was changed to high flow (NHFC). Low AOM activity was detected over the entire core after experiment termination with highest turnover between 7 and 9 cm sediment depth, while methane concentrations stayed continuously low around  $2\text{-}3 \mu\text{mol l}^{-1}$  over the entire core (see sampling artifacts, section 3.2.3.). In the HFC experiment, the SBTZ and related AOM activity was much more pronounced than in the LFC. The SBTZ moved upwards from 14 cm (max. depth) to  $<6 \text{ cm}$ , and dropped down to 10 cm sediment

Tina Treude 12.8.2015 18:50

**Gelöscht:** (before and after fluid flow change)

Tina Treude 13.8.2015 15:01

**Gelöscht:** 1080

Tina Treude 13.8.2015 15:01

**Gelöscht:** 108

Tina Treude 13.8.2015 16:34

**Gelöscht:** i.e.,

Tina Treude 12.8.2015 17:59

**Gelöscht:** and bromide

588 depth during the subsequent low flow phase (NLFC). During the first phase, fluids and SBTZ showed  
589 continuous migration, which was fast initially and became slower towards the end. The relatively  
590 stable depth of the SBTZ at the end of the first experiment phase (0 - 260 d) indicated the transition  
591 to a quasi-steady state situation. Highest AOM rates, determined by radiotracer measurements after  
592 experiment termination, were found within this SBTZ (6 - 10 cm sediment depth).

593 Sulfide concentrations of the HFC were generally highest within the SBTZ. In the LFC experiment,  
594 sulfide peaks were relatively broad and not so distinct, which was probably the result of a broad  
595 dispersive mixing layer between seepage and seawater medium. Due to the low fluid flow, higher  
596 sulfide concentrations evolved in the LFC as compared to the HFC, where sulfide was probably  
597 flushed-out before it accumulated. Relatively low sulfide concentrations were also observed at  
598 Mound 11, a seep site with high AOM and sulfate reduction activity and high fluid flow (Hensen et al.  
599 2004; Krause et al. 2014). In the LFC experiments, sulfide concentrations fluctuated over time. While  
600 the increase in sulfide concentration was most likely correlated with enhanced sulfate reduction, a  
601 decrease could be caused either by the precipitation of metal sulfides and/or by microbial oxidation  
602 of sulfide (chemosynthesis). Precipitation of metal sulfides is correlated with a drop in pH (Glud et al.  
603 2007; Preisler et al. 2007), as it was observed in our study. Oxygen and nitrate are important electron  
604 acceptors for microbial oxidation of sulfide in seep habitats. However, free oxygen was probably  
605 available only temporally (if at all) in the overlying water of the core due to a sampling artifact (see  
606 results), which was in accordance with a redox potential of less than 300 mV (Schulz 2000).

607 Moreover, sulfide oxidation with oxygen would create a drop in pH. Conversely, pH increased in the  
608 surface sediment, which could be caused by sulfide oxidation via dissimilatory nitrate reduction to  
609 ammonium. The process has been previously observed at the sediment-water interface of seeps  
610 system (de Beer et al. 2006). Nitrate availability in the seawater medium was limited ( $\sim 4 \mu\text{mol l}^{-1}$ ).  
611 Nevertheless, sulfide-oxidizing bacteria, such as *Beggiatoa* or *Thioploca* can accumulate nitrate in  
612 their vacuoles (Fossing et al. 1995; Preisler et al. 2007). Furthermore, sediment cores recovered from  
613 the field were covered by sulfide-oxidizing bacterial mats. Since oxygen concentration in the bottom

614 water was extremely low in this OMZ ( $< 22 \mu\text{mol l}^{-1}$ , Wyrтки 1962; Levin 2003), nitrate appears to be  
615 the most attractive electron acceptor for these sulfide oxidizers.

616 In summary, the observed increase in sulfide concentrations was most likely attributed to sulfate  
617 reduction activity, according to the development of the SBTZ. A loss of sulfide was caused by  
618 porewater flushing through advection, which was most pronounced in the HFC. Sulfide loss via  
619 oxidation with nitrate (top of the sediment) and sulfide precipitation (below 2 cm sediment depth)  
620 occurred more likely in the LFC.

#### 621 4.2 Microbial turnover rates and efficiency of the benthic methane filter

622 [Table 5 provides an overview of parameters \(fluid flow, methane emission, methane flux, AOM rate\)](#)

623 [from different methane seep locations](#). Integrated areal AOM rates ( $45.15 \pm 11.48 \text{ mmol m}^{-2} \text{ d}^{-1}$ ) of

624 [ex situ radiotracer measurements from the present study](#) were in the upper range of previous

625 modeled data ( $1.5 - 42.1 \text{ mmol m}^{-2} \text{ d}^{-1}$  [Karaca et al. 2012](#)) and moderate to high compared to other

626 seep systems (Treude et al. 2003; Joye et al. 2004; Niemann et al. 2006; Knittel and Boetius 2009;

627 Krause et al. 2014). In the SLOT experiments, the calculated methane flux ( $0.3 - 2.8 \text{ mmol m}^{-2} \text{ d}^{-1}$ )

628 was lower compared to modeled flux ( $9.1 - 41.7 \text{ mmol m}^{-2} \text{ d}^{-1}$ ) of the replicate core and at the lower

629 limit of the previously modeled data ( $0.2 - 56.1 \text{ mmol m}^{-2} \text{ d}^{-1}$ , [Karaca et al. 2012](#)). However, fluxes of

630 the SLOT experiment were still in the range of data published for seeps in this region (Mau et al.

631 2006; Karaca et al. 2010). In agreement with the relatively low methane flux during the SLOT

632 experiment, AOM rates (determined from the difference in methane concentration between in and

633 outflow) were 1 to 2 orders of magnitude lower compared to ex situ determinations. AOM rates

634 determined with radiotracer measurements after experiment termination revealed peaks within the

635 SBTZ (proxy for the SMTZ) of the HFC (4 - 10 cmbsf). A broader distribution of AOM was found in the

636 LFC, while similar integrated rates suggest the same potential for AOM. This agreement of integrated

637 AOM rates despite differences in fluid flux illustrates a widening of the AOM zone with lower fluid

638 fluxes, while a narrow AOM zone at high fluxes appears to be compensated by higher methane

639 turnover. This effect was also reflected in a more distinct peak of sulfide (see above) and confirmed

Tina Treude 11.8.2015 19:10

**Gelöscht:** the

Tina Treude 10.8.2015 17:03

**Gelöscht:** 2.6

Tina Treude 10.8.2015 17:04

**Gelöscht:** 5.1

Tina Treude 10.8.2015 17:04

**Gelöscht:** 1.5

Tina Treude 10.8.2015 17:04

**Gelöscht:** 8.0

645 by simulations in the numerical model, specifically at the two model runs from SO206-31 (MUC) (Fig.  
646 1 and 2). However, it should be kept in mind that methane concentrations during the experiment  
647 were much lower than under in situ pressure and it is therefore difficult to predict the upper limit of  
648 the balance between fluid flux and AOM activity.

649 While in a previous study the methane consumption efficiency of the benthic filter was estimated to  
650 range between 23 and 96% of the methane flux (Karaca et al. 2012), the efficiency in our study was

651 between 92 and 100% in the modeled ex situ data and 99% for the SLOT setup. The latter value is  
652 based on the assumption that steady-state conditions were reached in the SLOT cores directly before  
653 fluid flow change, which was most likely reached in the HFC, but not in the LFC (see discussion  
654 above). A reason for the partial disagreement in efficiency of the benthic filter compared to the  
655 earlier studies could be the natural variability of methane fluxes in this highly heterogeneous area.

656 While Karaca et al. (2012) based their results on a large number of sediment cores (20 cores from the  
657 same seep site), only two randomly chosen sites were sampled in our study, and only one was used  
658 for the experiment. Another explanation could be temporal variability of fluid and methane flux.

659 Karaca et al. (2012) conducted their study 10 years prior to ours. Methane flux as well as microbial  
660 activity could have changed easily over this period (Mau et al. 2007; Furi et al. 2010). A drop in  
661 methane flux would probably enhance the efficiency of the benthic methane filter. For example, in  
662 the present experiment, methane fluxes were 2 to 33 times lower compared to the model of Karaca  
663 et al. (2012) since the system was not pressurized and hence the solubility of methane was limited.  
664 Lower methane fluxes resulted in a high efficiency of the benthic microbial methane filter, despite  
665 relatively high fluid advection.

666 Radiotracer determination of microbial turnover rates after the experiment revealed sulfate  
667 reduction activity at levels higher than AOM, which was probably partly coupled to organic matter  
668 degradation. Since the cores were obtained within an oxygen minimum zone, sulfate reduction is  
669 supposedly the most important pathway for organic matter degradation (Jørgensen 1977; Sørensen  
670 et al. 1979; Bohlen et al. 2011). High C/N ratios in cores of the terminated experiment compared to

Tina Treude 12.8.2015 13:56  
**Gelöscht:** expected than

Tina Treude 12.8.2015 19:03  
**Gelöscht:** experimental

Tina Treude 12.8.2015 16:19  
**Gelöscht:** (under

Tina Treude 12.8.2015 16:20  
**Gelöscht:** of

Tina Treude 12.8.2015 16:20  
**Gelöscht:** )

676 ex situ cores (Fig. 8 and 9) support this assumption, because advanced microbial degradation of fresh  
677 organic matter with high nitrogen content leads to a shift from low to high C/N ratios (Whiticar  
678 2002). We assume that at most 80% of the sulfate reduction in the ex situ analyses of SO206-St31  
679 (MUC) can be related to organic matter degradation (AOM : SR = 0.21). Most likely, this ratio was  
680 less, because ex situ radiotracer incubations were conducted under atmospheric pressure and less  
681 methane was available compared to the in situ conditions. However, because organoclastic sulfate  
682 reduction occurred ex situ at the sediment-water interface (0 - 2 cmbsf, Fig. 1 and 2), where the  
683 consumed sulfate is replenished relatively rapidly by diffusion and mixing from the seawater, this  
684 surface activity has probably only little effect on sulfate gradients deeper in the sediment (Jørgensen  
685 et al. 2001; Karaca et al. 2012).

686 In Summary, the benthic microbial methane filter at Quepos Slide was found to be very efficient  
687 under continuous flow. Only increases in fluid and methane flux, such as at the beginning of the  
688 experiment or more pronounced after the fluid flow change, led to a drop in efficiency. Once a new  
689 steady state situation establishes, higher fluxes are expected to be compensated by a more intensive  
690 AOM zone (see above).

#### 691 4.3 Response time of the microbial benthic methane filter:

692 In the outflow of the LFC, methane concentrations increased only little and decreased after 202 d  
693 (directly before fluid flow change) to the initial concentration. In contrast, methane concentrations in  
694 the outflow of the HFC core were high ( $7.5 \mu\text{mol l}^{-1}$ ) at the beginning (29 d) and decreased quasi-  
695 exponentially to concentrations of  $\sim 2 \mu\text{mol l}^{-1}$  after 171 d. In the same time interval, the fraction of  
696 the methane-containing "seepage" medium at the sediment-water interface, calculated from the  
697 tracer (bromide) concentrations, changed from 13% to 34%, (Fig. 4 A, J). From the delivered methane  
698 ( $125.5$  and  $376.4 \mu\text{mol l}^{-1}$ ) 30% and 98%, was oxidized after 29 and 171 d, respectively, in the HFC.  
699 This period (0-171 d) can be interpreted as the response time of the benthic microbial methane filter  
700 in the sediments of Quepos Slide. After change of the flow regime, the efflux of methane suddenly  
701 reduced to only 22% ( $0.009 \text{ mmol m}^{-2} \text{ d}^{-1}$ ) in the former HFC (=NLFC), while the efflux in the former

Tina Treude 12.8.2015 13:59

**Gelöscht:** around

Tina Treude 12.8.2015 13:59

**Gelöscht:** was probably

Tina Treude 12.8.2015 13:59

**Gelöscht:** Admittedly, this ratio was likely overestimated

Tina Treude 12.8.2015 14:01

**Gelöscht:** its

707 LFC (=NHFC) increased rapidly 15-fold ( $0.169\text{mmol m}^{-2} \text{d}^{-1}$ ) after changing the fluid flow. Based on  
708 bromide concentrations, the fraction of seepage medium in the outflow of the NHFC was 4%, which  
709 should theoretically equal  $38.5 \mu\text{mol l}^{-1}$  methane in the outflow, if no methane would be consumed.  
710 Compared to methane concentrations directly measured in the outflow, only ~70% of the inflow  
711 methane was oxidized and 30% was emitted.

712 These results illustrate how sudden events could result in an abrupt increase in methane efflux. Mau  
713 et al. (2006) attributed fluctuations of methane concentrations in the water column, which occurred  
714 between autumn 2002 and 2003 at the Costa Rican seeps, to an earthquake in June 2002. However,  
715 it was not specified if the increased methane flux resulted from increased fluid flow, or simply from  
716 bubble release or if it was a continuous increase of methane flux or just a transient effect.

717 The experiments of the present study clearly show that the benthic microbial methane filter is able  
718 to respond within a relatively brief time of 5-6 months to increased methane fluxes and leads to the  
719 development of a much shallower and thinner AOM zone. Even if methane fluxes and methane  
720 concentrations were four times higher in situ, as expected from modeled methane fluxes of this  
721 study, the benthic microbial methane filter may still be able to respond quickly if a methanotrophic  
722 community is already fully established. Outside of seep habitats, where the microbial benthic  
723 methane filter is either absent or in deeper sediment zones, the adaptation might require much  
724 more time, since the doubling rate of the microbes involved is in the order of a few months (Girguis  
725 et al. 2005; Nauhaus et al. 2007; Krüger et al. 2008; Meulepas et al. 2009). Mau et al. (2007)  
726 observed a reduction of methane emissions in the water column above the earthquake-impacted  
727 seepage area by 50-90% in a period of one year. In our experiments, the benthic microbial methane  
728 filter required only ~170 d to adapt to the new flow regime. It is not clear, if the subsequent  
729 reduction of methane emissions observed by Mau et al. (2007) was the result of an ephemeral pulse  
730 of methane flux or by the adaption of the microbial benthic methane filter. Our results indicate that  
731 at least both situations are conceivable.

732 Another scenario, in which the benthic methane filter would be challenged, is the destabilization of  
733 gas hydrates as a result of climate change (Buffett and Archer 2004). However, due to retarded heat  
734 flux into deeper sediment layers, dissociation of considerable gas hydrate volumes probably require  
735 hundreds to thousands of years (Biastoch et al. 2011). In the present study, we demonstrate that an  
736 established microbial benthic methane filter can compensate relatively abrupt increases in methane  
737 flux. Only "pristine" sediments, which are virtually devoid of methanotrophs are expected to show  
738 long adaptations periods of up to several years or even decades (Dale et al. 2008) due to slow growth  
739 rates of the anaerobes (Girguis et al. 2005; Nauhaus et al. 2007; Goffredi et al. 2008).

Tina Treude 12.8.2015 14:13

**Gelöscht:** slow,

## 5. Conclusions:

Surface sediments of the Quepos Slide, a cold seep on the Pacific coastline of Costa Rica located within the Eastern Tropical North Pacific oxygen minimum zone, feature a very efficient benthic methane filter, demonstrated by direct measurements of methane turnover rates ex situ and numerical reaction modeling. In vitro experiments with intact sediment cores using a sediment-flow-through system further allowed following the adaptation of the SMTZ to changes in fluid flow, which revealed that the SMTZ narrows to a thin layer under high fluid flow conditions. Methane (ca. 1 mmol L<sup>-1</sup> at atmospheric pressure) transported under high fluid flow was efficiently consumed (99% oxidation) by the benthic methane filter after a response period of ca. 170 d. These results illustrate how an established benthic methanotrophic microbial community could react to pulses in fluid and methane flow induced, for example, by earthquakes or gas hydrate dissociation, and how it regains its efficiency level after passing through a non-steady state period. As we here present only one example of a response to a sudden fluid flow pulse, further studies from other seep systems are advisable to validate our results.

Tina Treude 11.8.2015 18:06

**Gelöscht:** highly

Tina Treude 11.8.2015 18:05

**Gelöscht:** which was confirmed

Tina Treude 11.8.2015 18:04

**Gelöscht:** (1)

Tina Treude 11.8.2015 18:04

**Gelöscht:** , (2) a

Tina Treude 11.8.2015 18:04

**Gelöscht:** , and (3) i

Tina Treude 11.8.2015 18:05

**Gelöscht:** . The flow-through system

Tina Treude 11.8.2015 18:05

**Gelöscht:** showing

Tina Treude 11.8.2015 18:08

**Formatiert:** Hochgestellt

Tina Treude 11.8.2015 18:08

**Gelöscht:** (but at atmospheric pressure)

Tina Treude 11.8.2015 18:11

**Gelöscht:** 150 –

767

768 **Author contribution:**

769 TT, PL, and CH initiated this study. PS, SK, MN, AD, sampled the sediment. SK and PS performed the  
770 radiotracer incubations. On board, AD was responsible for porewater measurements and MN  
771 conducted the methane measurements. CH and PS carried out the numerical modeling with input  
772 from AD. SK and PS carried out rate measurements and turnover calculations. Experiments were  
773 designed by TT and PL. Experiments were performed by PS including measurements and calculations.  
774 PS wrote the manuscript with input TT, PL, and AD as well as other co-authors.

775

776 **Acknowledgments:**

777 We thank the captain and the crew of R/V *SONNE* and all staff members who this supported work  
778 onboard. Special thanks goes to B. Domeyer, A. Bleyer, R. Ebbinghaus, R. Surberg, E. Corrales-  
779 Cordero, and E. Pinero for technical support during porewater analyzes. K. Kretschmer is thanked for  
780 help during maintenance of the SLOT-system. K. Kretschmer, J. Farkas, and J. Hommer are thanked for  
781 technical support during radiotracer analyzes. [We thank three anonymous referees and P. Dando for](#)  
782 [their helpful comments on the submitted manuscript.](#) This project was financed through the  
783 Collaborative Research Center (SFB) 574 "Volatiles and Fluids in Subduction Zones" and the Cluster of  
784 Excellence "The Future Ocean" funded by the German Research Foundation (DFG). M. Nuzzo was  
785 funded by the Portuguese Science and Technology Foundation post-doctoral fellowship FCT-  
786 SFRH/BPD/44598/2008.

787

788 **References:**

- 789 Aiello, I. W. 2005. Fossil seep structures of the Monterey Bay region and tectonic/structural controls  
790 on fluid flow in an active transform margin. *Palaeogeogr. Palaeoclimatol. Palaeoecol.* **227**: 124–  
791 142.
- 792 De Beer, D., E. Sauter, H. Niemann, N. Kaul, U. Witte, M. Schlüter, and A. Boetius. 2006. In situ fluxes  
793 and zonation of microbial activity in surface sediments of the Håkon Mosby Mud Volcano.  
794 *Limnol. Oceanogr.* **51**: 1315–1331.
- 795 Biastoch, A., T. Treude, L. H. Rüpke, U. Riebesell, C. Roth, E. B. Burwicz, W. Park, M. Latif, C. W.  
796 Böning, G. Madec, and K. Wallmann. 2011. Rising Arctic Ocean temperatures cause gas hydrate  
797 destabilization and ocean acidification. *Geophys. Res. Lett.* **38**: 1–5.
- 798 Boetius, A., K. Ravensschlag, C. J. Schubert, D. Rickert, F. Widdel, A. Gieseke, R. Amann, B. B.  
799 Jørgensen, U. Witte, O. Pfannkuche, and B. B. Jørgensen. 2000. A marine microbial consortium  
800 apparently mediating anaerobic oxidation of methane. *Nature* **407**: 623–626.
- 801 Bohlen, L., A. W. Dale, S. Sommer, T. Mosch, C. Hensen, A. Noffke, F. Scholz, and K. Wallmann. 2011.  
802 Benthic nitrogen cycling traversing the Peruvian oxygen minimum zone. *Geochim. Cosmochim.*  
803 *Acta* **75**: 6094–6111.
- 804 Bohrmann, G., K. Heeschen, C. Jung, W. Weinrebe, B. Baranov, R. Heath, V. Hu, M. Hort, and D.  
805 Masson. 2002. Widespread fluid expulsion along the seafloor of the Costa Rica convergent  
806 margin. *Terra Nov.* **14**: 69–79.
- 807 Borowski, W. S., C. K. Paull, and W. Ussler III. 1996. Marine pore-water sulfate profiles indicate in situ  
808 methane flux from underlying gas hydrate. *Geology* **24**: 655–658.
- 809 Borowski, W. S., C. K. Paull, and W. Ussler III. 1999. Global and local variations of interstitial sulfate  
810 gradients in deep-water, continental margin sediments: Sensitivity to underlying methane and  
811 gas hydrates. *Mar. Geol.* **159**: 131–154.
- 812 Buffett, B., and D. Archer. 2004. Global inventory of methane clathrate: sensitivity to changes in the  
813 deep ocean. *Earth Planet. Sci. Lett.* **227**: 185–199.
- 814 Burwicz, E., L. Rüpke, and K. Wallmann. 2011. Estimation of the global amount of submarine gas  
815 hydrates formed via microbial methane formation based on numerical reaction-transport  
816 modeling and a novel parameterization of Holocene sedimentation. *Geochim. Cosmochim. Acta*  
817 **75**: 4562–4576.
- 818 Cline, J. 1969. Spectrophotometric determination of hydrogen sulfide in natural waters. *Limnol.*  
819 *Oceanogr.* **14**: 454–458.
- 820 Crutchley, G. J., D. Klaeschen, L. Planert, J. Bialas, C. Berndt, C. Papenberg, C. Hensen, M. J. Hornbach,  
821 S. Krastel, and W. Brueckmann. 2014. The impact of fluid advection on gas hydrate stability:  
822 Investigations at sites of methane seepage offshore Costa Rica. *Earth Planet. Sci. Lett.* **401**: 95–  
823 109.

- 824 Dale, A. W., V. Brüchert, M. Alperin, and P. Regnier. 2009. An integrated sulfur isotope model for  
825 Namibian shelf sediments. *Geochim. Cosmochim. Acta* **73**: 1924–1944.
- 826 Dale, A. W., P. Van Cappellen, D. R. Aguilera, and P. Regnier. 2008. Methane efflux from marine  
827 sediments in passive and active margins: Estimations from bioenergetic reaction–transport  
828 simulations. *Earth Planet. Sci. Lett.* **265**: 329–344.
- 829 Dalsgaard, T., L. P. Nielsen, V. Brotas, P. Viaroli, G. Underwood, D. Nedwell, K. Sundbäck, S. Rysgaard,  
830 A. Miles, M. Bartoli, L. Dong, D. C. O. Thornton, L. D. M. Ottosen, G. Castaldelli, and N. Risgaard-  
831 Petersen. 2000. Sediment Characteristics, p. 53–54. *In* Protocol Handbook for NICE- Nitrogen  
832 Cycling in Estuaries: a project under EU research programme: Marine Science and Technology  
833 (MAST III). National Environmental Research Institute.
- 834 Ettwig, K. F., M. K. Butler, D. Le Paslier, E. Pelletier, S. Manganot, M. M. M. Kuypers, F. Schreiber, B. E.  
835 Dutilh, J. Zedelius, D. de Beer, J. Gloerich, H. J. C. T. Wessels, T. van Alen, F. Luesken, M. L. Wu,  
836 K. T. van de Pas-Schoonen, H. J. M. Op den Camp, E. M. Janssen-Megens, K.-J. Francoijs, H.  
837 Stunnenberg, J. Weissenbach, M. S. M. Jetten, and M. Strous. 2010. Nitrite-driven anaerobic  
838 methane oxidation by oxygenic bacteria. *Nature* **464**: 543–8.
- 839 Fischer, D., J. M. Mogollón, M. Strasser, T. Pape, G. Bohrmann, N. Fekete, V. Spiess, and S. Kasten.  
840 2013. Subduction zone earthquake as potential trigger of submarine hydrocarbon seepage. *Nat.*  
841 *Geosci.* **6**: 647–651.
- 842 Fischer, D., H. Sahling, and K. Nöthen. 2012. Interaction between hydrocarbon seepage,  
843 chemosynthetic communities, and bottom water redox at cold seeps of the Makran  
844 accretionary prism: insights from habitat-specific pore water sampling and modeling.  
845 *Biogeochemistry* **9**: 2013–2031.
- 846 Fossing, H., V. Gallardo, B. Jørgensen, M. Hüttel, L. P. Nielson, H. Schulz, D. E. Canfield, S. Forster, R.  
847 N. Glud, J. K. Gundersen, J. Küver, N. B. Ramsing, A. Teske, B. Thamdrup, and O. Ulloa. 1995.  
848 Concentration and transport of nitrate by the mat-forming sulphur bacterium *Thioploca*. *Nature*  
849 **374**: 714–715.
- 850 Furi, E., D. R. Hilton, M. D. Tryon, K. M. Brown, G. M. McMurtry, W. Brückmann, and C. G. Wheat.  
851 2010. Carbon release from submarine seeps at the Costa Rica fore arc: Implications for the  
852 volatile cycle at the Central America convergent margin. *Geochemistry, Geophys. Geosystems*  
853 **11**, doi:10.1029/2009GC002810
- 854 Girguis, P., A. Cozen, and E. DeLong. 2005. Growth and population dynamics of anaerobic methane-  
855 oxidizing archaea and sulfate-reducing bacteria in a continuous-flow bioreactor. *Appl. Environ.*  
856 *Microbiol.* **71**: 3725–3733.
- 857 Glud, R. N., P. Berg, H. Fossing, and B. B. Jørgensen. 2007. Effect of the diffusive boundary layer on  
858 benthic mineralization and O<sub>2</sub> distribution: A theoretical model analysis. *Limnol. Oceanogr.* **52**:  
859 547–557.
- 860 Goffredi, S. K., R. Wilpiseski, R. Lee, and V. J. Orphan. 2008. Temporal evolution of methane cycling  
861 and phylogenetic diversity of archaea in sediments from a deep-sea whale-fall in Monterey  
862 Canyon, California. *ISME J.* **2**: 204–20.

- 863 Haese, R.R., C. Meile, P.V. Cappellen, G.J. De Lange. 2003. Carbon geochemistry of cold seeps:  
864 methane fluxes and transformation in sediments from Kazan mud volcano, eastern  
865 Mediterranean Sea, *Earth Planet. Sci. Lett.* **212**: 361–375.
- 866 Han, X., E. Suess, H. Sahling, and K. Wallmann. 2004. Fluid venting activity on the Costa Rica margin:  
867 new results from authigenic carbonates. *Int. J. Earth Sci.* **93**: 596–611.
- 868 Harders, R., C. R. Ranero, W. Weinrebe, and J. H. Behrmann. 2011. Submarine slope failures along the  
869 convergent continental margin of the Middle America Trench. *Geochemistry Geophys.*  
870 *Geosystems* **12**, doi:10.1029/2010GC003401
- 871 Henrys, S., M. Reyners, I. Pecher, S. Bannister, Y. Nishimura, and G. Maslen. 2006. Kinking of the  
872 subducting slab by escalator normal faulting beneath the North Island of New Zealand. *Geology*  
873 **34**: 777.
- 874 Hensen, C., and K. Wallmann. 2005. Methane formation at Costa Rica continental margin—  
875 constraints for gas hydrate inventories and cross-décollement fluid flow. *Earth Planet. Sci. Lett.*  
876 **236**: 41–60.
- 877 Hensen, C., K. Wallmann, M. Schmidt, C. R. Ranero, and E. Suess. 2004. Fluid expulsion related to  
878 mud extrusion off Costa Rica—A window to the subducting slab. *Geology* **32**: 201.
- 879 Hesse, R., S. K. Frape, P. K. Egeberg, and R. Matsumoto. 2000. Stable Isotope Studies (Cl, O, and H) of  
880 Interstitial Waters from Site 997, Blake Ridge Gas Hydrate Field, West Atlantic. *Proc. Ocean Drill.*  
881 *Program, Sci. results* **164**: 129–137.
- 882 Hinrichs, K., and A. Boetius. 2002. The anaerobic oxidation of methane: new insights in microbial  
883 ecology and biogeochemistry, p. 457–477. *In* G. Wefer, D. Billet, D. Hebbeln, B. Jørgensen, M.  
884 Schlüter, and T. Van Weering [eds.], *Ocean Margin Systems*. Springer-Verlag Berlin Heidelberg.
- 885 Ivanenkov, V. N., and Y. I. Lyakhin. 1978. Determination of total alkalinity in seawater, p. 110–114. *In*  
886 O.K. Bordovsky and V.N. Ivanenkov [eds.], *Methods of Hydrochemical Investigations in the*  
887 *Ocean*. Nauka Publ. House.
- 888 Jørgensen, B. B. 1977. The Sulfur Cycle of a Coastal Marine Sediment (Limfjorden, Denmark). *Limnol.*  
889 *Oceanogr.* **22**: 814–832.
- 890 Jørgensen, B. B. 1978. A comparison of methods for the quantification of bacterial sulfate reduction  
891 in coastal marine sediments. 1. Measurements with radiotracer techniques. *Geomicrobiol. J* **1**:  
892 11–27.
- 893 Jørgensen, B., A. Weber, and J. Zopfi. 2001. Sulfate reduction and anaerobic methane oxidation in  
894 Black Sea sediments. *Deep Sea Res. Part I Oceanogr. Res. Pap.* **48**: 2097–2120.
- 895 Joye, S. B., A. Boetius, B. N. Orcutt, J. P. Montoya, H. N. Schulz, M. J. Erickson, and S. K. Lugo. 2004.  
896 The anaerobic oxidation of methane and sulfate reduction in sediments from Gulf of Mexico  
897 cold seeps. *Chem. Geol.* **205**: 219–238.
- 898 Judd, A., M. Hovland, and L. Dimitrov. 2002. The geological methane budget at continental margins  
899 and its influence on climate change. *Geofluids* **2**: 109–126.

- 900 Kallmeyer, J., T. G. Ferdelman, A. Weber, H. Fossing, and B. B. Jørgensen. 2004. A cold chromium  
901 distillation procedure for radiolabeled sulfide applied to sulfate reduction measurements.  
902 *Limnol. Oceanogr. Methods* **2**: 171–180.
- 903 Karaca, D., C. Hensen, and K. Wallmann. 2010. Controls on authigenic carbonate precipitation at cold  
904 seeps along the convergent margin off Costa Rica. *Geochemistry Geophys. Geosystems* **11**: 1–  
905 19.
- 906 Karaca, D., T. Schleicher, C. Hensen, P. Linke, and K. Wallmann. 2012. Quantification of methane  
907 emission from bacterial mat sites at Quepos Slide offshore Costa Rica. *Int. J. Earth Sci.* 1–25.
- 908 Kluesner, J. W., E. A. Silver, N. L. Bangs, K. D. McIntosh, J. Gibson, D. Orange, C. R. Ranero, and R. von  
909 Huene. 2013. High density of structurally controlled, shallow to deep water fluid seep indicators  
910 imaged offshore Costa Rica. *Geochemistry, Geophys. Geosystems* **14**: 519–539.
- 911 Knittel, K., and A. Boetius. 2009. Anaerobic oxidation of methane: progress with an unknown process.  
912 *Annu. Rev. Microbiol.* **63**: 311–34.
- 913 Krause, S., P. Steeb, C. Hensen, V. Liebetrau, A. W. Dale, M. Nuzzo, and T. Treude. 2014. Microbial  
914 activity and carbonate isotope signatures as a tool for identification of spatial differences in  
915 methane advection: a case study at the Pacific Costa Rican margin. *Biogeosciences* **11**: 507–523.
- 916 Krüger, M., M. Blumenberg, S. Kasten, A. Wieland, L. Känel, J. Klock, W. Michaelis, and R. Seifert.  
917 2008. A novel, multi-layered methanotrophic microbial mat system growing on the sediment of  
918 the Black Sea. *Environ. Microbiol.* **10**: 1934–47.
- 919 Kutterolf, S., V. Liebetrau, T. Mörz, A. Freundt, T. Hammerich, and D. Garbe-Schönberg. 2008.  
920 Lifetime and cyclicity of fluid venting at forearc mound structures determined by  
921 tephrostratigraphy and radiometric dating of authigenic carbonates. *Geology* **36**: 707.
- 922 Kvenvolden, K. 2002. Methane hydrate in the global organic carbon cycle. *Terra Nov.* **14**: 302–306.
- 923 Lein, A., P. Vogt, K. Crane, A. Egorov, M. Ivanov. 1999. Chemical and isotopic evidence for the nature  
924 of the fluid in CH<sub>4</sub>-containing sediments of the Hakon Mosby Mud Volcano, *Geo. Mar. Lett.* **19**:  
925 76–83.
- 926 Levin, L. A. 2003. Oxygen Minimum Zone Benthos : Adaption and Community. *Ocean. Mar. Biol. an*  
927 *Annu. Rev.* **41**: 1–45.
- 928 Linke, P., K. Wallmann, E. Suess, C. Hensen, and G. Rehder. 2005. In situ benthic fluxes from an  
929 intermittently active mud volcano at the Costa Rica convergent margin. *Earth Planet. Sci. Lett.*  
930 **235**: 79–95.
- 931 Mau, S., G. Rehder, I. G. Arroyo, J. Gossler, and E. Suess. 2007. Indications of a link between  
932 seismotectonics and CH<sub>4</sub> release from seeps off Costa Rica. *Geochemistry, Geophys.*  
933 *Geosystems* **8**: 1–13.
- 934 Mau, S., G. Rehder, H. Sahling, T. Schleicher, and P. Linke. 2012. Seepage of methane at Jaco Scar, a  
935 slide caused by seamount subduction offshore Costa Rica. *Int. J. Earth Sci.* , doi:10.1007/s00531-  
936 012-0822-z

- 937 Mau, S., H. Sahling, G. Rehder, E. Suess, P. Linke, and E. Soeding. 2006. Estimates of methane output  
938 from mud extrusions at the erosive convergent margin off Costa Rica. *Mar. Geol.* **225**: 129–144.
- 939 Meulepas, R. J. W., C. G. Jagersma, J. Gieteling, C. J. N. Buisman, A. J. M. Stams, and P. N. L. Lens.  
940 2009. Enrichment of anaerobic methanotrophs in sulfate-reducing membrane bioreactors.  
941 *Biotechnol. Bioeng.* **104**: 458–70.
- 942 Milucka, J., T. G. Ferdelman, L. Polerecky, D. Franzke, G. Wegener, M. Schmid, I. Lieberwirth, M.  
943 Wagner, F. Widdel, and M. M. M. Kuypers. 2012. Zero-valent sulphur is a key intermediate in  
944 marine methane oxidation. *Nature* **2**: 1–23.
- 945 Minami, H., K. Tatsumi, A. Hachikubo, S. Yamashita, H. Sakagami, N. Takahashi, H. Shoji, Y. K. Jin, A.  
946 Obzhirov, N. Nikolaeva, and A. Derkachev. 2012. Possible variation in methane flux caused by  
947 gas hydrate formation on the northeastern continental slope off Sakhalin Island, Russia. *Geo-*  
948 *Marine Lett.* **32**: 525–534.
- 949 Nauhaus, K., M. Albrecht, M. Elvert, A. Boetius, and F. Widdel. 2007. In vitro cell growth of marine  
950 archaeal-bacterial consortia during anaerobic oxidation of methane with sulfate. *Environ.*  
951 *Microbiol.* **9**: 187–96.
- 952 Niemann, H., T. Lösekann, D. de Beer, M. Elvert, T. Nadalig, K. Knittel, R. Amann, E. J. Sauter, M.  
953 Schlüter, M. Klages, J. P. Foucher, and A. Boetius. 2006. Novel microbial communities of the  
954 Haakon Mosby mud volcano and their role as a methane sink. *Nature* **443**: 854–8.
- 955 Orcutt, B. N., J. B. Sylvan, N. J. Knab, and K. J. Edwards. 2011. Microbial ecology of the dark ocean  
956 above, at, and below the seafloor. *Microbiol. Mol. Biol. Rev.* **75**: 361–422.
- 957 Pimenov, N., A. Savvichev, I. Rusanov, A. Lein, A. Egorov, A. Gebruk, L. Moskalev, P. Vogt. 1999.  
958 Microbial processes of carbon cycle as the base of food chain of Hakon Mosby Mud Volcano  
959 benthic community, *Geo Mar. Lett.* **19**: 89–96.
- 960 Preisler, A., D. de Beer, A. Lichtschlag, G. Lavik, A. Boetius, and B. B. Jørgensen. 2007. Biological and  
961 chemical sulfide oxidation in a Beggiatoa inhabited marine sediment. *ISME J.* **1**: 341–53.
- 962 Ranero, C., and R. von Huene. 2000. Subduction erosion along the Middle America convergent  
963 margin. *Nature* **404**: 748–52.
- 964 Ranero, C. R., I. Grevemeyer, H. Sahling, U. Barckhausen, C. Hensen, K. Wallmann, W. Weinrebe, P.  
965 Vannucchi, R. von Huene, and K. McIntosh. 2008. Hydrogeological system of erosional  
966 convergent margins and its influence on tectonics and interplate seismogenesis. *Geochemistry*  
967 *Geophys. Geosystems* **9**, doi:10.1029/2007GC001679
- 968 Reeburgh, W. S. 2007. Oceanic methane biogeochemistry. *Chem. Rev.* **107**: 486–513.
- 969 Sahling, H., D. G. Masson, C. R. Ranero, V. Hühnerbach, W. Weinrebe, I. Klaucke, D. Bürk, W.  
970 Brückmann, and E. Suess. 2008. Fluid seepage at the continental margin offshore Costa Rica and  
971 southern Nicaragua. *Geochemistry, Geophys. Geosystems* **9**: 1–22.
- 972 Sahling, H., D. Rickert, R. W. Lee, P. Linke, and E. Suess. 2002. Macrofaunal community structure and  
973 sulfide flux at gas hydrate deposits from the Cascadia convergent margin, NE Pacific. *Mar. Ecol.*  
974 *Prog. Ser.* **231**: 121–138.

- 975 Schmidt, M., C. Hensen, T. Mörz, C. Müller, I. Grevemeyer, K. Wallmann, S. Mau, and N. Kaul. 2005.  
976 Methane hydrate accumulation in "Mound 11" mud volcano, Costa Rica forearc. *Mar. Geol.*  
977 **216**: 83–100.
- 978 Schulz, H. D. 2000. Redox Measurements in Marine Sediments, p. 235–246. *In* J. Schüring, H.D.  
979 Schulz, J. Böttcher, and W.H.M. Duijnsveld [eds.], REDOX: Fundamentals, Processes, and  
980 Applications. Springer Berlin.
- 981 Sørensen, J., B. Jørgensen, and N. Revsbech. 1979. A comparison of oxygen, nitrate, and sulfate  
982 respiration in coastal marine sediments. *Microb. Ecol.* **5**: 105–115.
- 983 Sommer, S., O. Pfannkuche, P. Linke, R. Luff, J. Greinert, M. Drews, S. Gubsch, M. Pieper, M. Poser, T.  
984 Viergutz. 2006. Efficiency of the benthic filter: Biological control of the emission of dissolved  
985 methane from sediments hosting shallow gas hydrates at Hydrate Ridge. *Global Biogeochem.*  
986 *Cycles* **20**: GB2019, doi:10.1029/2004GB002389
- 987 Steeb, P., P. Linke, and T. Treude. 2014. A sediment flow-through system to study the impact of  
988 shifting fluid and methane flow regimes on the efficiency of the benthic methane filter. *Limnol.*  
989 *Oceanogr. Methods* **12**: 25–45.
- 990 Suess, E. 2010. Marine Cold Seeps, p. 188–198. *In* K.N. Timmis [ed.], Handbook of Hydrocarbon and  
991 Lipid Microbiology. Springer Berlin Heidelberg.
- 992 Syracuse, E. M., and G. a. Abers. 2006. Global compilation of variations in slab depth beneath arc  
993 volcanoes and implications. *Geochemistry, Geophys. Geosystems* **7**: 1–18.
- 994 Tishchenko, P., C. Hensen, K. Wallmann, and C. S. Wong. 2005. Calculation of the stability and  
995 solubility of methane hydrate in seawater. *Chem. Geol.* **219**: 37–52.
- 996 Torres, M. E. E., K. Wallmann, A. M. M. Tréhu, G. Bohrmann, W. S. Borowski, and H. Tomaru. 2004.  
997 Gas hydrate growth, methane transport, and chloride enrichment at the southern summit of  
998 Hydrate Ridge, Cascadia margin off Oregon. *Earth Planet. Sci. Lett.* **226**: 168–175.
- 999 Torres, M. E., J. McManus, D. E. Hammond, M. A. de Angelis, K. U. Heeschen, S. L. Colbert, M. D.  
1000 Tryon, K. M. Brown, and E. Suess. 2002. Fluid and chemical fluxes in and out of sediments  
1001 hosting methane hydrate deposits on Hydrate Ridge, OR, I: Hydrological provinces. *Earth Planet.*  
1002 *Sci. Lett.* **201**: 525–540.
- 1003 Treude, T., A. Boetius, K. Knittel, K. Wallmann, and B. Barker Jørgensen. 2003. Anaerobic oxidation of  
1004 methane above gas hydrates at Hydrate Ridge, NE Pacific Ocean. *Mar. Ecol. Prog. Ser.* **264**: 1–  
1005 14.
- 1006 Treude, T., M. Krüger, A. Boetius, and B. Jørgensen. 2005. Environmental control on anaerobic  
1007 oxidation of methane in the gassy sediments of Eckernförde Bay(German Baltic). *Limnol.*  
1008 *Oceanogr.* **50**: 1771–1786.
- 1009 Tryon, M. D., K. M. Brown, and M. E. Torres. 2002. Fluid and chemical fluxes in and out of sediments  
1010 hosting methane hydrate deposits on Hydrate Ridge, OR, II: Hydrological provinces. *Earth*  
1011 *Planet. Sci. Lett.* **201**: 541–557.
- 1012 Tryon, M. D., C. G. Wheat, and D. R. Hilton. 2010. Fluid sources and pathways of the Costa Rica  
1013 erosional convergent margin. *Geochemistry, Geophys. Geosystems* **11**: n/a–n/a.

- 1014 Visser, W., W. A. Scheffers, W. H. Batenburg-van der Vegte, and J. P. van Dijken. 1990. Oxygen  
1015 requirements of yeasts. *Appl. Environ. Microbiol.* **56**: 3785–3792.
- 1016 Wallmann, K., M. Drews, G. Aliosi, G. Bohrmann. 2006. Methane discharge into the Black Sea and the  
1017 global ocean via fluid flow through submarine mud volcanoes. *Earth Plan. Sci. Lett.* **248**: 545-560.
- 1018 Wallmann, K., E. Pinero, E. Burwicz, M. Haeckel, C. Hensen, A. Dale, and L. Ruepke. 2012. The Global  
1019 Inventory of Methane Hydrate in Marine Sediments: A Theoretical Approach. *Energies* **5**: 2449–  
1020 2498.
- 1021 Wankel, S. D., M. M. Adams, D. T. Johnston, C. M. Hansel, S. B. Joye, and P. R. Girguis. 2012.  
1022 Anaerobic methane oxidation in metalliferous hydrothermal sediments: influence on carbon  
1023 flux and decoupling from sulfate reduction. *Environ. Microbiol.* **14**: 2726–40.
- 1024 Whiticar, M. J. 2002. Diagenetic relationships of methanogenesis , nutrients, acoustic turbidity ,  
1025 pockmarks and freshwater seepages in Eckernförde Bay. *Mar. Geol.* **182**: 29–53.
- 1026 Widdel, F., and F. Bak. 2006. Gram-negative mesophilic sulfate-reducing bacteria, p. 3352–3378. *In*  
1027 M. Dworkin, S. Falkow, E. Rosenberg, K.-H. Schleifer, and E. Stackebrandt [eds.], *The*  
1028 *Prokaryotes*. Springer US.
- 1029 Wyrtki, K. 1962. The oxygen minima in relation to ocean circulation. *Deep. Res.* **9**: 11–23.
- 1030

1031 **Figure Captions:**

1032 Figure 1: Depth profiles of measured and modeled porewater parameters and microbial turnover  
1033 rates for SO206-29 (MUC), sampled from 402 m water depth. A) measured (diamonds) and modeled  
1034 (thick green line) sulfate concentrations (per L porewater), as well as measured (circles) and modeled  
1035 (thick blue line) methane concentrations (per L sediment), (B) three replicates (thin lines and  
1036 symbols) of measured sulfate reduction rates (per cm<sup>-3</sup> sediment), C) three replicates of measured  
1037 (thin lines and symbols) and modeled (thick line) AOM rates (per cm<sup>-3</sup> sediment), D) measured  
1038 (triangles) and modeled sulfide concentration (thick orange line), measured (squares) and modeled  
1039 (thick grey line) total alkalinity (per L porewater).

Tina Treude 13.8.2015 16:48

**Gelöscht:** as well as

Tina Treude 13.8.2015 14:33

**Formatiert:** Hochgestellt

Tina Treude 11.8.2015 14:54

**Gelöscht:** AOM rates

Tina Treude 13.8.2015 12:55

**Gelöscht:** (thick line)

1041 Figure 2: Depth profiles of measured and modeled porewater parameters and microbial turnover  
1042 rates for SO206-31 (MUC) sampled from 401 m water depth. Thick solid lines = pw-fit model, thick  
1043 dashed lines = hf-fit model (for details see Results). A) measured (diamonds) and modeled (thick  
1044 green lines) sulfate concentrations (per L porewater), measured (circles) and modeled (thick blue  
1045 lines) methane concentrations (per L sediment), B) three replicates (thin lines and symbols) of  
1046 measured sulfate reduction rates (per cm<sup>-3</sup> sediment), C) three replicates of measured (thin lines and  
1047 symbols) and modeled (thick lines) AOM rates (per cm<sup>-3</sup> sediment), D) measured (triangles) and  
1048 modeled (thick orange lines) sulfide concentration, measured (squares) and modeled (thick grey  
1049 lines) total alkalinity (per L porewater).

Tina Treude 13.8.2015 12:53

**Gelöscht:** as well as

Tina Treude 13.8.2015 12:46

**Gelöscht:** as well as

Tina Treude 13.8.2015 12:51

**Gelöscht:** for the porewater fit (solid lines) and higher fluid flow fitted for the rate core (dashed lines)

Tina Treude 13.8.2015 14:35

**Gelöscht:**

Tina Treude 12.8.2015 12:34

**Gelöscht:** AOM rates

Tina Treude 13.8.2015 12:27

**Gelöscht:** AOM rates

Tina Treude 12.8.2015 12:34

**Gelöscht:** for the porewater fit (solid line) and higher fluid flow fitted for the rate core (dashed line)

Tina Treude 13.8.2015 12:52

**Gelöscht:** (orange lines)

Tina Treude 13.8.2015 12:53

**Gelöscht:** for the porewater fit (solid lines) and higher fluid flow of the rate cores (dashed lines)

1051 Figure 3: Sulfate and bromide concentrations (left panel), sulfide and total alkalinity concentrations  
1052 (middle panel), redox potential and pH (right panel) measured in the sediment of the low flow  
1053 regime core (LFC) from Quepos Slide after different days of runtime indicated on the left. All  
1054 concentrations are presented per L porewater. Please consider the different scales for sulfide  
1055 concentrations.

1076 Figure 4: Sulfate and bromide concentrations (left panel), sulfide and total alkalinity concentrations  
1077 (middle panel), redox potential and pH (right panel) measured in the sediment of the high flow  
1078 regime core (HFC) from Quepos Slide after days of runtime indicated on the left. The SBTZ as proxy  
1079 for the SMTZ is highlighted by the grey bar. All concentrations are presented per L porewater. Please  
1080 consider the different scales for sulfide concentrations.  
1081

1082 Figure 5: Methane concentration ( $\mu\text{mol l}^{-1}$ ) in the outflow (A, D), methane efflux ( $\text{mmol m}^{-2} \text{d}^{-1}$ ; B, E),  
1083 and calculated AOM rate ( $\text{mmol m}^{-2} \text{d}^{-1}$ ; C, F) of the SLOT system before and after changing the fluid  
1084 flow regime: (A, B, C) low flow regime core (LFC), and (D, E, F) high flow regime core (HFC) from  
1085 Quepos Slide. Vertical lines mark the moment of fluid flow change (low flow  $\rightarrow$  high flow and vice  
1086 versa at 258 d runtime). Error bars (A, D) show standard deviations of three repeated gas  
1087 chromatographic measurements; the first two data points represent single measurements. Dotted  
1088 lines represent the trendline (low flow regime:  $5 \times 10^{-6} * t_{\text{runtime}}^2 + 0.02 t_{\text{runtime}} + 0.285$ ,  $r^2 = 0.825$ ; high  
1089 flow regime:  $0.8576 * \ln(t_{\text{runtime}}) - 0.8662$ ,  $r^2 = 0.987$ ) of methane concentration development until  
1090 flow change.  
1091

1092 Figure 6: Solute concentrations and turnover rates in the new high flow core (NHFC) after experiment  
1093 termination (358 d runtime). Porewater profiles of methane (A, crosses), sulfate (B, crosses), sulfide  
1094 (C, circles), and results of the radiotracer measurements for AOM (A, bars) and sulfate reduction (B,  
1095 bars) are shown.  
1096

1097 Figure 7: Solute concentrations and turnover rates in the new low flow core (NLFC) after experiment  
1098 termination (358 d runtime). Porewater profiles of methane (A, crosses), sulfate (B, crosses), sulfide  
1099 (C, circles), and results of the radiotracer measurements for AOM (A, bars) and sulfate reduction (B,  
1100 bars) are shown.  
1101

Tina Treude 10.8.2015 17:06

**Gelöscht: B**

Tina Treude 10.8.2015 17:06

**Gelöscht: C,D**

Tina Treude 10.8.2015 17:06

**Gelöscht: E**

Tina Treude 10.8.2015 17:06

**Gelöscht: , E**

Tina Treude 10.8.2015 17:06

**Gelöscht: B,**

Tina Treude 13.8.2015 16:50

**Gelöscht: Selected**

Tina Treude 13.8.2015 16:50

**Gelöscht: Selected**

1109 Figure 8: Sediment solid phase parameters measured in the sediment of the ex situ replicate SO206-  
1110 31 (MUC) core (grey lines and symbols) compared to the NHFC (original LFC, black lines and symbols).  
1111 Total carbon content (TC, diamonds), and total inorganic carbon content (TIC, circles) in dry wt.% (A);  
1112 atomic C/N ratio (circle) and total organic carbon content (TOC, triangles) in dry wt.% (B); total  
1113 nitrogen (TN, diamonds), total sulfur (TS, circles) in dry wt.% (C); porosity of the sediment (D).

1114

1115 Figure 9: Sediment solid phase parameters measured in the sediment of the ex situ replicate of the  
1116 SO206-31 (MUC) core (grey lines and symbols) compared to the NLFC (original HFC, black lines and  
1117 symbols). Total carbon content (TC, diamonds), and total inorganic carbon content (TIC, circle) in dry  
1118 wt.% (A); atomic C/N ratio (circle) and total organic carbon content (TOC, triangles) in dry wt.% (B);  
1119 total nitrogen (TN, diamonds), total sulfur (TS, circles) in dry wt.% (C); porosity of the sediment (D).

1120

1121

1122

1123 **Tables:**

1124 Table 1: Sampling sites of the Quepos Slide and the SMTZ depth in cm below seafloor (bsf).

Station	Latitude (N)	Longitude (W)	Water depth m	Depth of SMTZ cmbsf
SO206-29 (MUC)	8°51.29'	84°12.60'	402	12.5 - 22.5
SO206-31 (MUC)	8°51.12'	84°13.06'	399	5.0 - 15.0

1125

1126

1127 Table 2: Summary of input parameters used for the model simulations and major model results. For  
 1128 the SO206-31 (MUC) cores, two fits are provided, since the replicate core for porewater  
 1129 determinations (pw-fit) exhibited a lower fluid flow and deeper SMTZ than the core used for rate  
 1130 determinations (hf-fit), probably as a result of high fluid flow heterogeneity at the site (see  
 1131 discussion). [For more model details, see Krause et al. 2014.](#)

Tina Treude 11.8.2015 18:59

Gelöscht: 4

Parameter	SO206-29 (MUC)	SO206-31 (MUC) pw-fit	SO206-31 (MUC) hf-fit	Unit	Parameter source
<b>Model parameter values</b>					
Length core	32	44	44	cm	measured
Length of simulated column	80	80	50	cm	fitted
Number of model layers	160	200	200		set
Temperature	8	8	8	°C	measured
Salinity	35	35	35	PSU	measured
Pressure	41	41	41	bar	measured
Porosity at sediment surface	0.95	0.93	0.93		measured
Porosity at the base of the sediment core	0.75	0.70	0.70		measured
Porosity at infinity sediment depth	0.74	0.70	0.70		fitted
Attenuation coef. for porosity decrease with depth	0.04	0.04	0.04	cm <sup>-1</sup>	fitted
Burial velocity at depth	0.02	0.02	0.03	cm yr <sup>-1</sup>	fitted
Fluid flow at the sediment water interface	7	5	29	cm yr <sup>-1</sup>	fitted
Kinetic for AOM	200000	25000	100000	cm mmol <sup>-1</sup> yr <sup>-1</sup>	fitted
Kinetic constant for CaCO <sub>3</sub> precipitation	0	0	0	yr <sup>-1</sup>	fitted
Density of dry solids in sediment	2.5	2.5	2.5	g cm <sup>-3</sup>	assumed
Kinetic constant for TH <sub>2</sub> S removal from porewater	0.02	0.1	0.005	mmol cm <sup>-3</sup> yr <sup>-1</sup>	fitted
Attenuation coef. for decrease in TH <sub>2</sub> S removal rate	0.07	0.6	0.05	cm <sup>-1</sup>	fitted
Non-local mixing coefficient	1.5	0	80	yr <sup>-1</sup>	fitted
Depth of irrigated layer	15	0	2	cm	fitted
Width of irrigated layer	5	0	1.5	cm	fitted
<b>Porewater concentration upper/lower boundary</b>					
Bottom water / Bottom sediment SO <sub>4</sub> <sup>2-</sup>	28.00 / 0.00	27.00 / 0.00	27.00 / 0.00	mmol l <sup>-1</sup>	measured
Bottom water / Bottom sediment CH <sub>4</sub>	0.00 / 61.00	0.00 / 61.00	0.00 / 61.00	mmol l <sup>-1</sup>	calculated*
Bottom water / Bottom sediment Cl <sup>-</sup>	558.00 / 380.00	548.00 / 320.00	548.00 / 320.00	mmol l <sup>-1</sup>	measured
Bottom water / Bottom sediment HCO <sub>3</sub> <sup>-</sup>	2.30 / 10.00	4.00 / 15.00	4.00 / 15.00	mmol l <sup>-1</sup>	measured
Bottom water / Bottom sediment TH <sub>2</sub> S	0.00 / 0.00	0.03 / 0.00	0.03 / 0.00	mmol l <sup>-1</sup>	measured
<b>Model Results</b>					
Methane flux at sediment bottom	12.40	9.09	45.09	mmol m <sup>-2</sup> d <sup>-1</sup>	modeled
Methane efflux at sediment water interface	0.98	0.00	3.39	mmol m <sup>-2</sup> d <sup>-1</sup>	modeled
Percentage of consumed methane	91.53	100.00	92.46	%	modeled
Anaerobic oxidation of methane	11.35	9.09	41.69	mmol m <sup>-2</sup> d <sup>-1</sup>	modeled
<b>Measured turnover rates (radiotracer techniques)</b>					
Sulfate reduction (entire sediment depth)	13.38 ± 13.61	218.90 ± 159.80	218.90 ± 159.80	mmol m <sup>-2</sup> d <sup>-1</sup>	measured
AOM (entire sediment depth)	12.87 ± 5.98	45.15 ± 11.48	45.15 ± 11.48	mmol m <sup>-2</sup> d <sup>-1</sup>	measured

Tina Treude 11.8.2015 14:24

Gelöscht: Coefficient for tortuosity calculation ... [1]

Tina Treude 11.8.2015 14:25

Gelöscht: Density of pore ... [2]

\*Calculated after Tishchenko et al. 2005

Tina Treude 10.8.2015 17:08

Gelöscht: 2

Tina Treude 11.8.2015 14:28

Gelöscht:

1141 Table 3: Salt concentrations of the two different media used in the SLOT-system. Seawater medium  
1142 with sulfate was delivered from the top, seepage medium with methane and without sulfate from  
1143 the bottom. In the last line, the gas in the respective medium headspace is denoted.

Tina Treude 11.8.2015 18:59

Gelöscht: 2

Salts (all in mmol l <sup>-1</sup> )	Seawater medium (with	
	SO <sub>4</sub> <sup>2-</sup> )	Seepage medium (with CH <sub>4</sub> )*
KBr	0.006	0.756
KCl	8.05	8.05
CaCl <sub>2</sub> 2H <sub>2</sub> O	10.0	10.0
MgCl <sub>2</sub> 6H <sub>2</sub> O	27.9	55.5
MgSO <sub>2</sub> 7H <sub>2</sub> O	27.6	0.000
NaCl	451	451
<b>Medium headspace</b>	N <sub>2</sub>	CH <sub>4</sub>

\* FeSO<sub>4</sub> (trace element) was replaced by FeCl (compare Widdel and Bak 2006)

1144

1145

1146

1148 Table 4: Overview of conditions during SLOT experiments: methane concentration of the “seepage”  
 1149 medium, methane flux, advective flow, and pump rate in the low and high flow core as well as  
 1150 experimental phases and run times under the low and high flow regime. The length of the sediment  
 1151 cores was 15 (LFC) and 14 (HFC) cm.

Tina Treude 11.8.2015 18:59

Gelöscht: 3

	low flow regime	high flow regime
Methane in $\mu\text{mol l}^{-1}$ (seepage medium)	965 $\pm$ 180	
Methane flux* in $\text{mmol m}^{-2} \text{d}^{-1}$	0.28	2.81
Advective flow in $\text{cm yr}^{-1}$	10.6	106.3
Pumping rate $\mu\text{l min}^{-1}$ (seepage medium)	0.5	5
Hydrological Residence Time (HRT)	1080	108
<b>Experimental phase</b>	<b>total time</b>	<b>phase time</b>
Initial	-40 - 0	40
Phase 1	0 - 258	258
Phase 2	258 - 350	92

\*Calculated by the methane concentration of the seepage medium multiplied by the advective flow

1152

1153

1155 Table 5: Fluid flow, methane emissions, methane fluxes, and AOM rates determined in sediments

1156 from cold seep sites covered with sulfur bacteria mats.

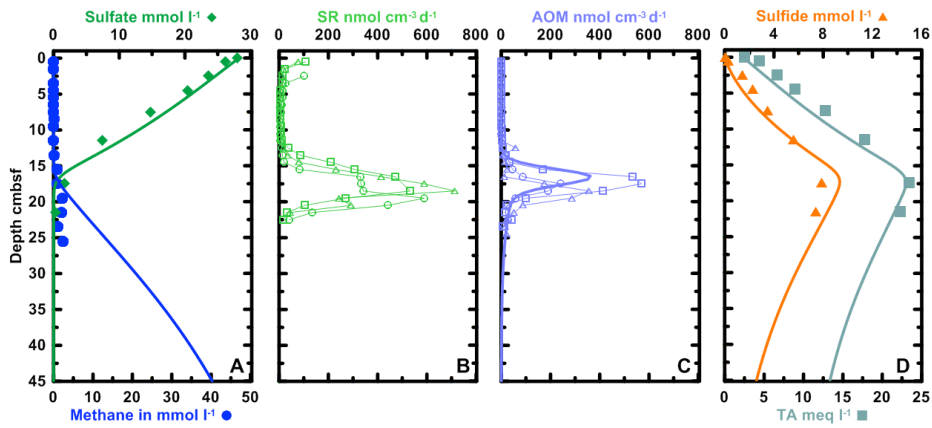
Cold seep sites with bacterial mats	Water depth (m)	Fluid flow (cm yr <sup>-1</sup> )	Methane emission (mmol m <sup>-2</sup> d <sup>-1</sup> )	Methane flux from depth (mmol m <sup>-2</sup> d <sup>-1</sup> )	Depth integrated AOM rate (mmol m <sup>-2</sup> d <sup>-1</sup> ) Max rate (nmol cm <sup>-3</sup> d <sup>-1</sup> )	Source
<b>Quepos Slide</b>						This study
SO206-29 (MUC)	402	7*	0.98*	12.4*	12.87 (0-32 cm)/11.35* (0-80 cm)	
SO206-31 (MUC) pw	399	5*	0.00*	9.09*	45.15 (0-44 cm)/9.09* (0-80 cm)	
SO206-31 (MUC) hf	399	29*	3.39*	45.09*	45.14 (0-44 cm)/41.69* (0-50 cm)	
LFC/NHFC	399	10.6	0.011-0.030/0.165	0.28	0.304*/2.970 (0-15 cm)*	
HFC/NLFC	399	106.3	0.025-0.109/0.009	2.81	3.114/0.306 (0-14 cm)	
<b>Quepos Slide</b>						Karaca et al. 2010
TV-MUC-63	406	40*	52.5*		58.4* (0-41.5 cm)	
TV-MUC-73	404	4*	20.2*		22.2* (0-32.5 cm)	
<b>Mound 11</b>	1024	200*/300* <sup>1</sup>	318.5*		9.6* (0-27.5 cm)	Hensen et al. 2004
<b>Culebra Fault</b>	1530	0.1*	0*		0.4* (0-810 cm)	
<b>Pockmark</b>	1917	3*	5.2*		9.2* (0-15 cm)	
<b>Quepos Slide</b>	397-410	1-40*	0.2-56.1*		1.5-42.1*	Karaca et al. 2012
<b>Mound 12</b>	1000	10*	0.01-3.8*/12.1*	28.3* (10 cm)	16.1* (0-10 cm)	Linke et al. 2005
<b>Mound 12</b>	1000	10	12.1-89.9		4.9-140.0	Mau et al. 2006
<b>Mound 11</b>						Krause et al. 2014
SO206-39	1005	200*	201.63*		140.71 (0-10 cm)/143.69* (0-100 cm)	
SO206-50	1003		0.30*		4.76 (0-270 cm)/1.62* (0-500 cm)	
<b>Mound 12</b>						
SO206-44	1007	15*	4.28*		22.37 (0-10 cm)/22.23* (0-100 cm)	
SO206-46	1009		12.45*		10.68 (0-10 cm)/16.16* (0-100 cm)	
<b>Green Canyon (Gulf of Mexico)</b> C4324	560				11.6 (0-13.5 cm) Max: 500 (13.5 cm)	Joye et al. 2004
C4315	540				4.61 (0-10.5 cm)	
<b>Hydrate Ridge (NE Pacific)</b>	777	10-250	30-100 <sup>2</sup>		99.0 (0-10 cm) Max: 5500 (8-9 cm)	Torres et al. 2002
	777		0.6-4*		15.1*	Treude et al. 2003
	778	20*	5.7 <sup>2</sup>	16.5* (20 cm)		Sommer et al. 2006
<b>Håkon Mosby mud volcano (North Atlantic)</b>	1250	250			0.55 (0-80 cm) Max: 0.8 (20-30 cm)	Pimenov et al. 1999
		30-60			6.7 (0-20 cm)	Lein et al. 1999
					12.32 (0-10 cm)	Niemann et al. 2006
<b>Kazan mud volcano (Mediterranean Sea)</b>	2000	3-5	0*	130 mM at depth		Haese et al. 2003
<b>Dvurechenskii mud volcano (Black Sea)</b>	2070	8-25*	3.4-11.1*	21.6-58.3*	16.7 (0-18 cm)/18.2-47.2* (0-26/38cm) Max: 563 (1 cm)	Wallmann et al. 2006

\*Model result, <sup>2</sup>benthic chamber/barrel measurement, <sup>1</sup>rate most likely overestimated as no steady state was reached.

1157

1158 **Figures:**

1159 **Figure 1:**



1160

1161

1162

Figure 2

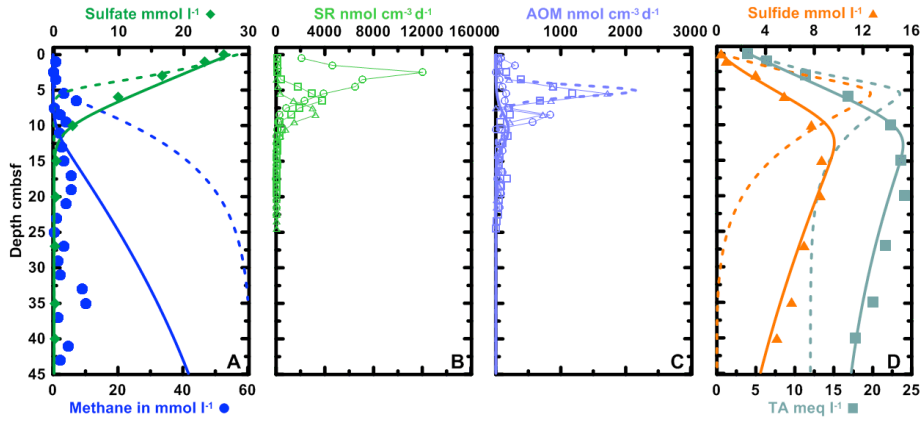


Figure 3

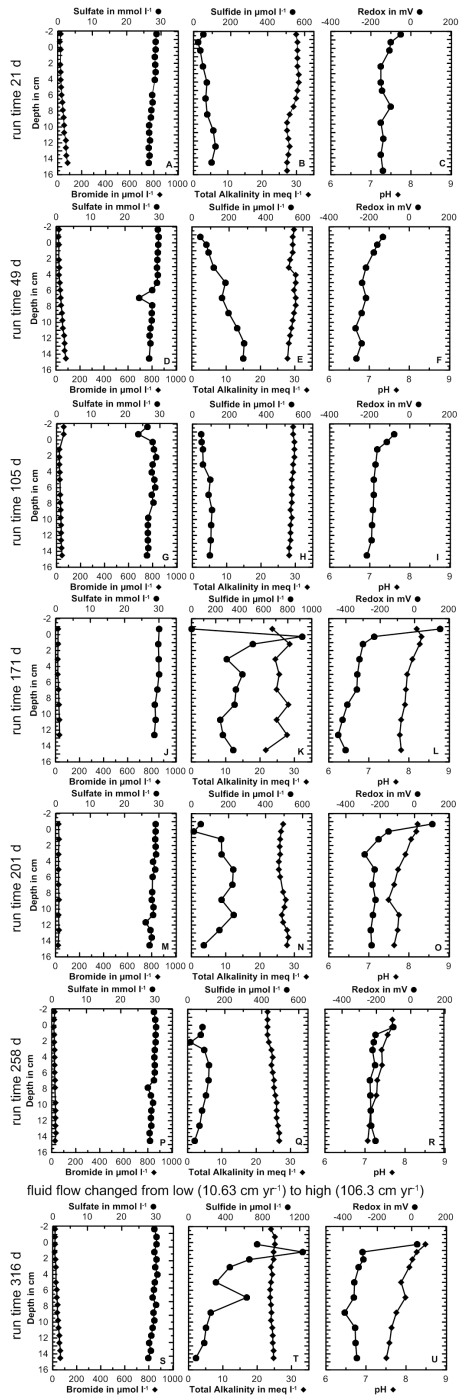
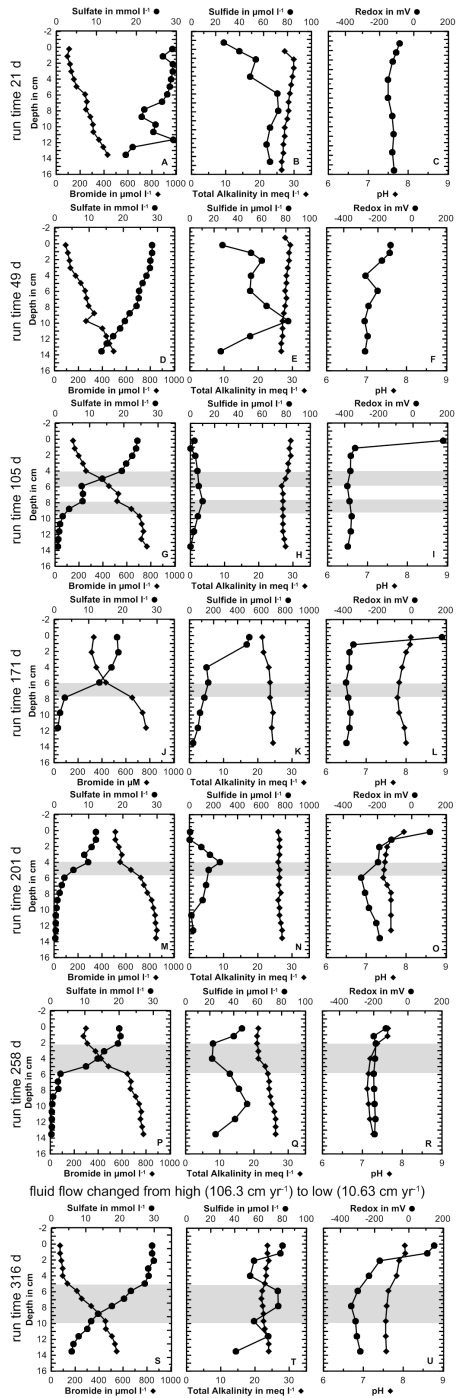
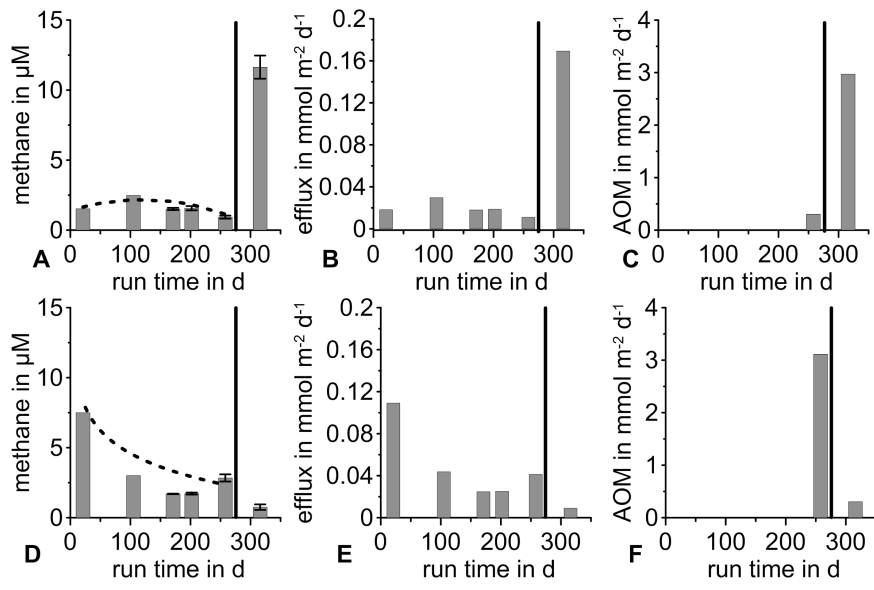


Figure 4



1171  
1172

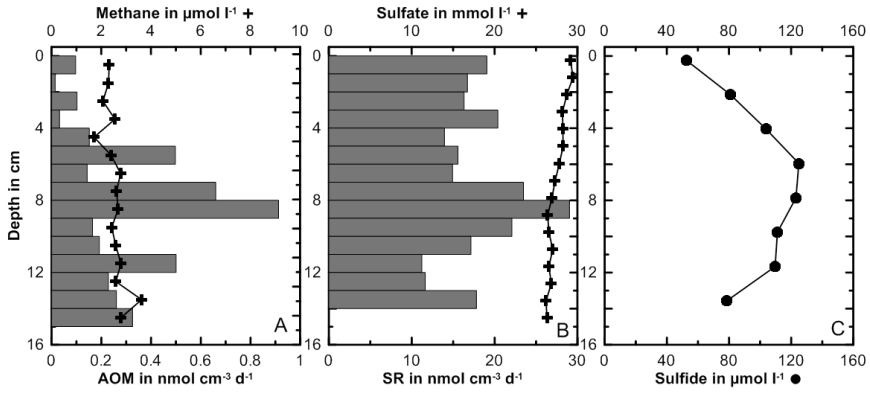
Figure 5



1173

1174

1175 **Figure 6**

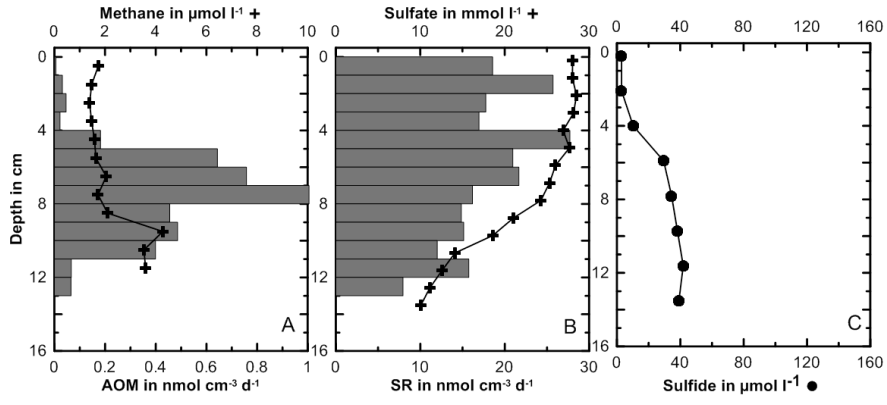


1176

1177

1178

Figure 7

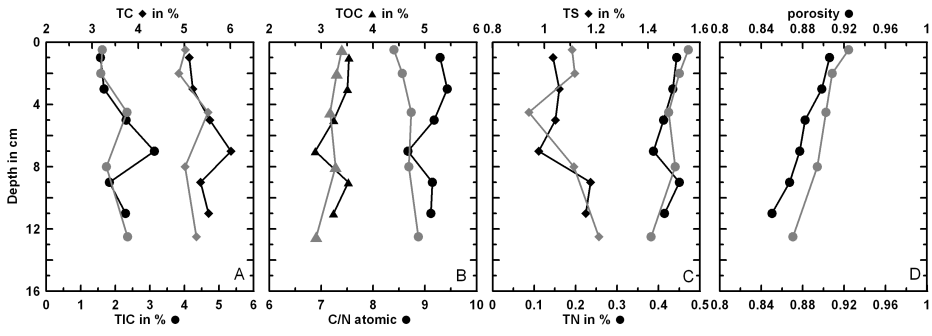


1179

1180

1181

Figure 8



1182

1183

Figure 9

